The Design and Fabrication of a Microfluidic Landscaper

by

Hoon Suk Rho

A thesis submitted to the Graduate Faculty of
Auburn University
in partial fulfillment of the
requirements for the Degree of
Master of Science

Auburn, Alabama
August 9, 2010

Keywords: Microfluidic, Micromixer, Enzyme reaction,
Landscaping, MMP-2

Approved by

Jong Wook Hong, Chair, Associate Professor of Materials Engineering
Jeffrey W. Fergus, Professor of Materials Engineering
Zhongyang Cheng, Associate Professor of Materials Engineering
Maria Auad, Assistant Professor of Polymer and Fiber Engineering

Abstract

Catalysis is identified as a feature of enzymes function, and kinetic analysis of the conversion generated by the reaction between proteins and enzymes is essential to understand and control them for biological applications. Due to the limitation of applying enzyme sequential and structural information for real catalytic behaviors and capabilities, new analysis tools are requested for the studies of new enzyme investigations. Therefore, novel integrated microfluidic systems for accurate and fast biocatalysts analysis could prompt to characterize enzyme catalysis with small reagent consumption required without sample preparation steps.

With the advantages of total analysis system in a single chip, an integrated microfluidic landscaper has been developed with an advantage of manipulating tiny sample volumes in nano/pico-liter scale and many different ratios of substrate, inhibitor, and buffer on a single chip for conducting enzyme binding kinetics. The microfluidic landscaper consists of forty five parallel processors, and each processor has designed to complete one set of enzyme reaction including metering, mixing, and detecting. This automated microfluidic landscaper system makes it possible to achieve the catalytic performances of an enzyme as a series of three-dimensional landscapes. This system would also provide a view of the catalytic ability of an enzyme with a complete understanding of the factors that have an effect on it and the indispensable information needed to obtain the constants governing their influences.

Acknowledgments

The author would like to acknowledge his deep and sincere gratitude towards his advisor Dr. Jong Wook Hong, for his immense support, patience and continuous encouragement. The author sincerely thankful to his committee members, Dr. Jeffrey W. Fergus, Dr. Zhongyang Cheng, and Dr. Maria Auad, for their invaluable guidance and helping during the course of this study. The author would like to thank Mr. Charles Ellis of Alabama Microelectronics Science and Technology Center (AMSTC) for permission to use the clean room for microfabrication.

The author would also like to express his deep gratitude and gratefulness to Dr. Duckjong Kim, Mr. Sachin Jambovane, and Dr. Jae Young Yoon, for passing on their knowledge and guidance during the course of this project. The author would also like to thank the company of his past and current research group members: Dr. Woon Seob Lee, Miss Hye Young Sim, Mr. Jing Dai, Mr. Jae Ha Woo, Miss Kirn Cramer, and Mr. Austin Adamson. The author would also like to thank to his family and friends, Dong Geun Rho, Yoon Ja Ae, Hyoung Suk Rho, Yoon Sun Yang, Christine Cooper, Chuck Cooper, Hudson Cooper, Ho Sang Ahn, Jung Hyun Park, Seon Bae Kim, Sang Hoon Yoon, Byoung Soo Kim, Jun Suk Kang, Tony Gnanaprakasa, Dong Liu, for their continuous love and support.

Table of Contents

List of Tables

List of Figures

CHAPTER 1
INTRODUCTION

1.1 Background

The microfluidic platforms are essential to the development of a miniaturized total analysis system due to their high number of advantages, including low sample and reagent consumptions, short response times, and ease of miniaturization (Auroux, Iossifidis et al. 2002; Vilkner, Janasek et al. 2004; Breslauer, Lee et al. 2006). Due to the concept of a total analysis system in a single chip, an automated microfluidic landscaper for enzyme binding kinetics at many different ratios of substrate and inhibitor is suggested in this proposal. The device consists of 45 microfluidic processors adapted to conventional experiments to analyze enzyme binding kinetics; hence highly integrated parallel processes of metering, concentration gradient generation, mixing, and optical detection have beec achieved simultaneously on this single chip. The characteristics of this automated microfluidic system are not only accurate and rapid analysis of enzyme binding kinetics according to the nano/picoliters of target enzyme and inhibitor, but also spontaneous and vivid three-dimensional output, which provides many advantages, including significant reduction in sample consumption, very short analysis time, and greater sensitivity for the biomedical and pharmaceutical applications.

1.2 Microfluidic platform for biology and biotechnology

The development of a silicon chip-based gas chromatography at Stanford University was a milestone in the history of modern microfluidics (Daw and Finkelstein 2006; Whitesides 2006). However, the concept of integrated and miniaturized microfluidic platforms, later called “lap on a chip,” was not fully developed until the early 1990s (Auroux, Iossifidis et al. 2002). Since this time, the microfluidics has flourished with the modification of the total analysis system approach by combining multiple analysis steps (sample preparation, reaction and detection) onto a single chip, with the advantages of fast response time, low sample and reagent consumptions, and automation (Reyes, Iossifidis et al. 2002). Due to the needs of small size device and the complexity of the applications in biological systems, the integrated and high-throughput microfluidic devices are employed to analyze biological elements, especially in terms of revealing their information related to the mechanisms of biological function (Emrich, Tian et al. 2002; Breslauer, Lee et al. 2006; Craighead 2006). After on-chip technologies to decode DNA sequences have succeeded, a large number of approaches in micro total analysis systems have been suggested and studied to address the genetic information of biological systems and to provide a complete map of the systems (Auroux, Iossifidis et al. 2002; Reyes, Iossifidis et al. 2002).

After the first successful fabrications of microvalves and micropumps by using micromachining technology at the end of the 1980s, many microfluidic components and platforms have been developed with novel micro fabrication technology for precise control of fluids in the microchannels (Xia and Whitesides 1998; Duffy, Gillis et al.

1999; McDonald, Duffy et al. 1999; Hruby 2001). Since PDMS (polydimethylsiloxane) was first suggested as the possible single elastomer material to realize microfluidic structures on a chip due to its powerful characteristics, such as good optical transparency and biocompatibility, monolithic fabrication for microfluidic components has become possible (Nguyen and Wereley 2002). With the merits of PDMS in the constructions of microfluidic components, the monolithic microfabrication technology based on the replication molding on micromachined molds also became possible. Moreover, the multilayer soft lithography, which was introduced by Stephen Quake's research group (Unger, Chou et al. 2000), made the precise control of fluid with pneumatic valves and pumps on a single chip possible(Hong, Studer et al. 2004; Jambovane, Duin et al. 2009).

1.3 Multilayer soft lithography

Since the introduction of multilayer soft lithography by Unger et al. (2000), This methodology has become one of the most popular in the field of microfluidics for the applications in biotechnology and nanotechnology. This technique combines soft lithography to achieve micro-molded elastomer layers, and then bonds the layers together. Enhanced with the merits of simplicity, strong adhesion between layers, and low internal thermal stress, up to seven patterned layers can be successfully fabricated using this technique. Figure 1.1 shows the schematic illustration of multilayer soft lithography by using silicon rubber.

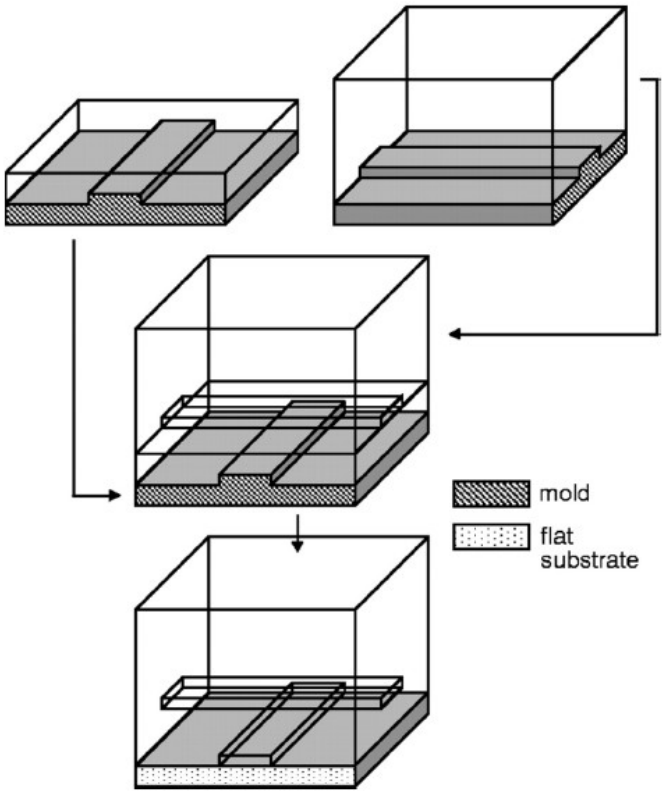

Figure 1.1 Schematic illustration of multilayer soft lithography
Source: [(Unger, Chou *et al.* 2000)]

The curing principle of the silicon rubber (GE RTV 615) in multi layer soft lithography is explained in Figure 1.2. The silicon rubber consists of two components: A and B. Component A contains a polydimethylsiloxane bearing vinyl groups and a platinum catalyst, and component B includes a cross-linker with silicon hydride group to perform covalent bonds with a polydimethylsiloxane bearing vinyl groups from component A, according to applied external thermal energy. Since the composition of each layer is designed to have an excess of specific components (e.g. the top layer has an excess of the component A, whereas the bottom layer has an excess of the component B), reactive molecules remain and form irreversible bonding at the interface of the top layer,

as well as the bottom layer. Designing the composition of silicon rubber for different layers, additional layers can be added one by one. Young's modulus of the elastomer – ~ 750 kPa – indicates the softness of the material. Consequently, the large deflection with small actuation can be achieved for the application of microfluidic platforms.

A. Chemical structure of polydimethylsiloxane

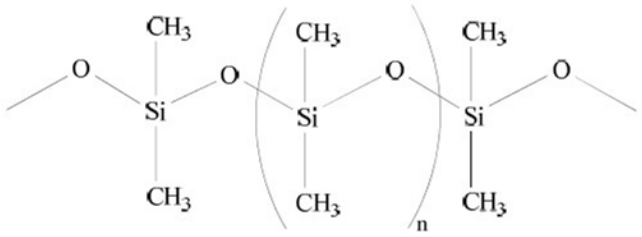

B. Mechanism of covalent bonding in two component addition-cure polydimethylsiloxane

$$-O(CH_3)Si-CH=CH_2+H-Si(CH_3)O-\xrightarrow{\Delta}-O(CH_3)Si-(CH_2)_2-Si(CH_3)O-$$

Figure 1.2 Curing principle of polydimethylsiloxane

1.4 Pneumatic control systems

1.4.1 Pneumatic valves

The pneumatic valve system is a key parameter in a microfluidic landscaper, to control the flow of reagents inside microchannels. The principle and geometry of the pneumatic valve system was developed by Quake and his research research group by using multilayer soft lithography (Unger, Chou et al. 2000). Utilizing the cross-channel architectures of two layers, two different types of microfluidic pneumatic valves were

fabricated in polydimethylsiloxane. When the upper layer acts as a control layer, the membrane deflects downward according to applied pressure, which is called ”push down geometry,” The opposite applies for ”push up geometry”, which means that a control layer is placed beneath a fluidic layer. Typically, a microchannel with 100 μm by 10 μm (channel width by channel height), and a membrane that has thickness between 10 μm to 30 μm, are used for the pneumatic microfluidic valve system. During the fabrication steps of a master mold for constructing a pneumatic microfluidic valve system, it is possible to obtain a rounded channel for a fluidic layer through reflowing photoresist at glass transition temperature. After this process, the height of the channel at the center increases with constant volume of a channel due to the balancing of surface tension. With the rounded fluidic channels, push up geometry can achieve reliable valve operations, with lower control pressure and thinner membrane than push down geometry. Figure 1.3 shows schematic of valve closing for push down and push up geometry. Schematic diagrams of single on-off valves in pneumatically controlled microfluidic systems are shown in figure 1.4.

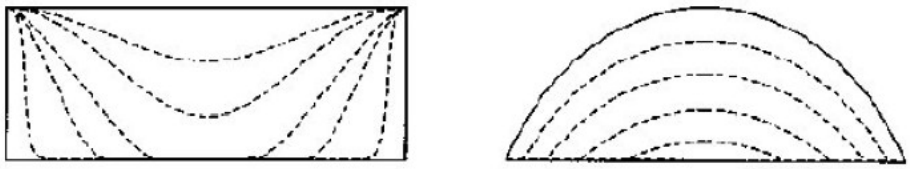

Figure 1.3 Schematic of valve operation in pneumatic microfluidic valve system. The dotted lines designate the contour of the membrane in push own geometry (left) and in push up geometry (right) according to applied pressure.
Source: [(Hadd, Jacobson et al. 1999; Unger, Chou et al. 2000; Seong, Heo et al.

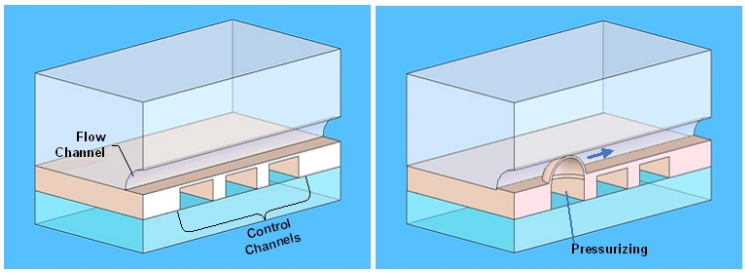

Figure 1.4 Schematic diagrams of an on-off valve in pneumatically controlled microfluidic system

1.4.2 Pneumatic mixer

Various microfluidic components have been implemented by the sequential control of the valves, and they can be easily integrated into a single chip (Chou, Unger et al. 2001; Nguyen and Wu 2005). First, it is introduced that plural adjoining valves can function as a peristaltic pump. Typically, three valves are placed in a series, and the air pressure for each valve is increased and released sequentially. Consequently, because of the sequential motion of the valves, fluid flow in the flow channel is generated. When this peristaltic pump operates in a loop, an active micromixer is created. For the peristaltic micromixers, multiple spots of one side of a ring-shaped microchannel are deflected sequentially by using a pneumatic control. This peristaltic motion generates fluid flow in the curved microchannel and, in the course of the flow, the interface between the fluids is stretched quickly, which significantly improves the mixing. In addition, the micromixer can hold the mixed reagents during analysis of the reaction. Due to the incubation capability of the micromixer, the reaction time can be flexibly controlled, and sample waste can be minimized. Figure 1.5 shows schematic diagrams of peristaltic microfluidic mixer in a pneumatic, control-based microfluidic system.

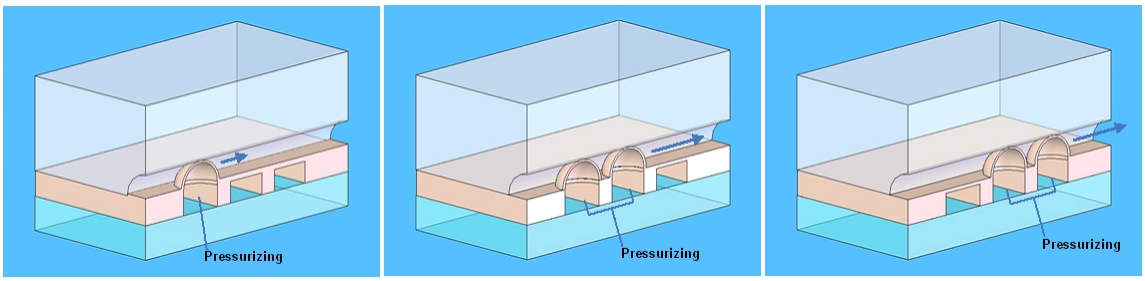

Figure 1.5 Schematic diagrams of peristaltic microfluidic mixer in pneumatic control-based microfluidic system

The possible operation sequence of pneumatically controlled peristaltic mixers was studied by Chou et al. (2001). Table 1.1 shows six sequences of valve operation for peristaltic fluidic motion in a microchannel. Through calculation of angular velocity of the fluid inside a ring-shaped micro reactor, it is known that the mixing time is directly proportional to the linear velocity of the fluid inside the reactor (see Figure 1.6).

Table 1.1 Sequence of valve operation for peristaltic motion in a microchannel

	Sequence #1	Sequence #2	Sequence #3	Sequence #4	Sequence #5	Sequence #6
Valve #1	On	On	Off	Off	Off	On
Valve #2	Off	On	On	On	Off	Off
Valve #3	Off	Off	Off	On	On	On

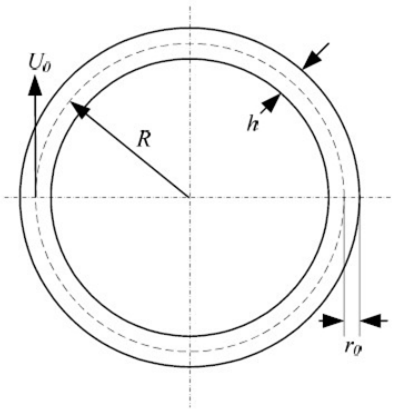

$$\omega_o = \frac{U_0}{R}\left[1-\left(\frac{r}{r_0}\right)^2\right]$$

U_0 = maximum velocity at the center of the channel

r_0 = Half of the width of the channel

R = Radius of the ring

Figure 1.6 Design parameters of pneumatically controlled micromixer
Source: [(Chou, Unger et al. 2001)]

1.5 Enzyme kinetics

The defining characteristic of an enzyme is its activity that is the catalytic conversion of substrates to the corresponding products (Palmer 1985). An enzyme mechanism proceeds by reversible association of the enzyme (E) and its substrate to form a complex ($E \cdot S$), which then generates the product (P). The reaction can be shown as follows.

$$E + S \underset{k_{-1}}{\longleftrightarrow} E \cdot S \xrightarrow{k_2} E + P$$

The first utilizing and characterizing enzyme kinetics experiment, Michaelis-Menten enzyme kinetics, was suggested by German biochemist Leonor Michaelis and Canadian medical scientist Maud Menten. This experiment imparts the quantitative measure of kinetics of enzyme, and Michaelis-Menten plot is drawn from the results of the experiment. The plot which provides enzyme kinetics is shown below in Figure 1.7.

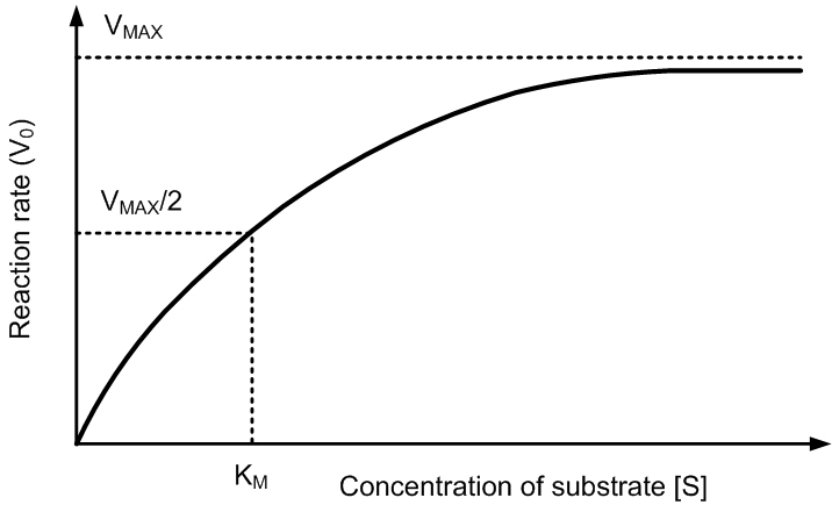

Figure 1.7 Michaelis-Menten plot
Source: [(Palmer 1985)]

The govern equation for this plot, Michaelis-Menten equation, is shown as

$$V_0 = V_{\max} \frac{[S]}{[S] + K_M}$$

Where [S] is the concentration of substrate, and K_M is Michaelis Constant.

Based on this mechanism, two essential parameters that govern enzyme rate as a function of substrate concentration were demonstrated. The k_{cat} (k_2 in reaction) describes the maximum catalytic turnover of the enzyme achieved when the substrate concentration is 'saturating'. That is, when dominant form of enzyme is $E \cdot S$. The Machaelis constant (K_M) is the concentration of substrate necessary to reach 1/2 the maximum output, and the according to the steady-state assumption of Briggs and Haldane, is given by $(k_1 + k_2)/k_1$. From these parameters, the apparent second-order rate constant governing catalysis (k_{app}) can be obtained; it is given by k_{cat}/K_M, a term

describing enzyme specificity and efficiency with a particular substrate.

The method of Dixon (1953) shows the inhibitor constant, K_i, that is the equilibrium constant of the reversible combination of an enzyme with a competitive inhibitor, which is obtained by calculation from Michaelis-Menten equation for a competitive system.

$$v = \frac{v_{\max}[S]}{K_m\left(1+\frac{[I]}{K_i}\right)+[S]\left(1+\frac{[I]}{K_i^*}\right)},$$

in which $[I]$, K_i, and K_i^* represent inhibitor concentration, the competitive inhibition constant and uncompetitive constant. In the case of competitive inhibition, the uncompetitive constant K_i^* is negligible and in uncompetitive inhibition the competitive constant K_i is negligible. In noncompetitive inhibition K_i and K_i^* are equal. Cornish-Bowden (1973) presented a graphical method for determination of inhibition constants of all cases including competitive inhibition, uncompetitive inhibition, and non-competitive inhibition based on the Dixon's method.

From the Dixon's method, $[S]/v$ against $[I]$ can be plotted as a straight line through following equation:

$$\frac{[S]}{v} = \frac{K_m}{v_{\max}}\left(1+\frac{[I]}{K_i}\right)+\frac{[S]}{v_{\max}}\left(1+\frac{[I]}{K_i^*}\right)$$

Thus, both K_i and K_i^* are simply measured at the intersections of the two Dixon's plots, $[I]=-K_i$ and $[S]/v = K_m[1-(K_i/K_i^*)]/v_{\max}$. Therefore, the half maximal

inhibitory concentration (IC_{50}) as well as the enzyme inhibition constants can be obtained by measuring the influence of $[I]$ and $[S]$ on the reaction rate.

1.6 Scope of the study

The objective of this study is to develop a highly integrated microfluidic system to accomplish protein kinetics experiments for generating landscapers. The integrated microfluidic device will allow reagents and samples' handling, metering, mixing, heating and optical detection, with 45 highly parallel processors on a single chip. With the collection of the data analyzed with the microfluidic system, not only determination of enzyme's general kinetic parameters will be achieved, but also their dependence on parameters, such as the concentration of an inhibitor or pH that can be achieved simultaneously. Moreover, the sample and reagent consumptions required are very low, with a nanoliter scale in each processor, and the repeated experiments can be accomplished through washing and drying processes. To produce this device, two detailed aims are proposed:

1. Design and fabricate microfluidic chips to analyze numerous enzyme reactions under the influence of different parameters.

2. Automate and integrate operation of the device, temperature control, and optical detection.

CHAPTER 2
LITERATURE REVIEW

2.1 Introduction

For the applications of the enzyme kinetics or enzyme inhibition kinetics in the fields of biochemistry and pharmaceuticals, small needs of reagents, automation, and fast analysis are critical requirements (Auroux, Iossifidis et al. 2002; Reyes, Iossifidis et al. 2002; Daw and Finkelstein 2006; Whitesides 2006). Thus, the tedious and time-consuming conventional method, including metering reagents by using pipets and mixing mechanically the reagent in a test tube or multi-well plate, is limited to reveal real-time enzymatic reactions (Breslauer, Lee et al. 2006). With the advantages of microreactors, including low sample and time consumption, integration and automation, several different microplatforms have been presented for the study of enzyme kinetics and enzyme inhibition kinetics.

2.2 Electrokinetically controlled microfluidics

Hadd et al. (1997) showed the possibility of conducting an enzyme reaction within a microfabricated channel network using electrokinetic flow (See Figure 2.1). Specific concentrations of substrate, enzyme, and inhibitor were mixed by using electrokinetic

flow and their reaction was monitored through laser-induced fluorescent on a chip. Michaelis-Menten constants that well matched with that from a conventional enzyme assay were derived by on-chip reactions with pico-grams of reagent. They expanded their microchip to the enzyme inhibition study by adding a separation procedure (Hadd, Jacobson et al. 1999). With the merits of low sample and time consumptions in a microchip, inhibitory behaviors of competitive and irreversible inhibitors were monitored and related inhibition constants were calculated.

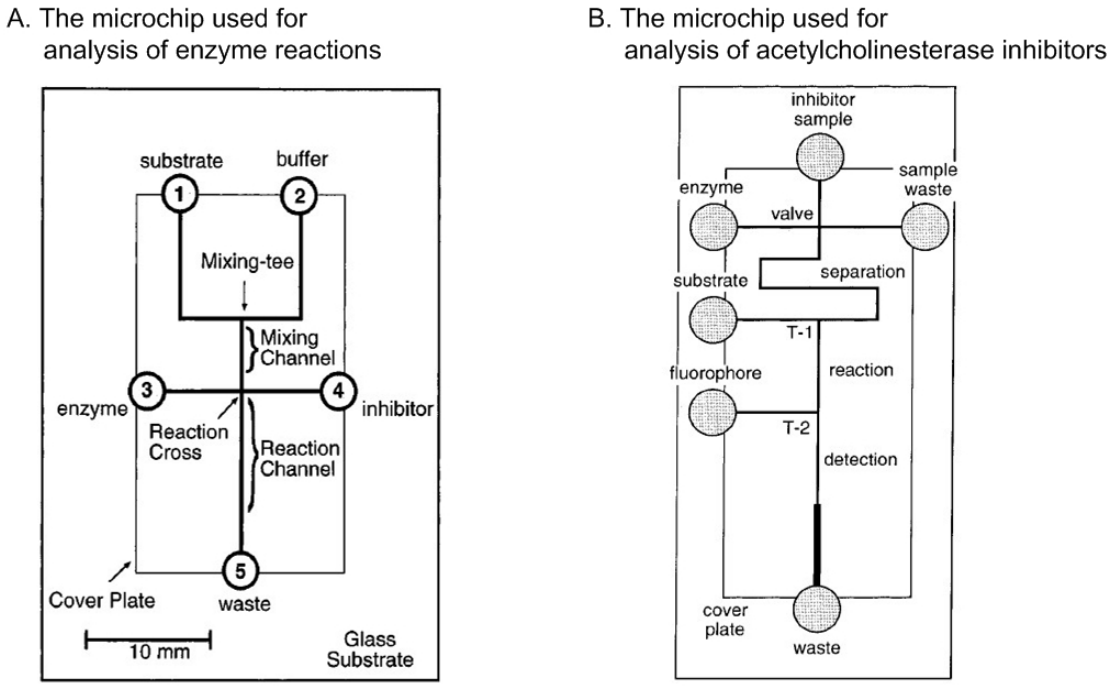

Figure 2.1 Design microchip used for analysis of enzyme kinetics (left) and enzyme inhibition kinetics (right).
Source: [(Hadd, Raymond et al. 1997; Hadd, Jacobson et al. 1999)]

Jacobson et al (1999) presented microfabricated platforms for parallel and serial mixing of fluids inside microchannels by using electrokinetically driven flows. With a

series of independent T-intersections, sample fractions of 1.0, 0.36, 0.21, 0.12, and 0.06 were generated for the parallel mixing device. Figure 1.2 shows the schematic design of the chip for serial electrokinetic mixing and test results of the chip with fluorescent molecules. From the results of performing serial mixing of fluids in the chip, it is shown that the parallel reactions could be conducted by using eletrokinetic flow inside a microchannel.

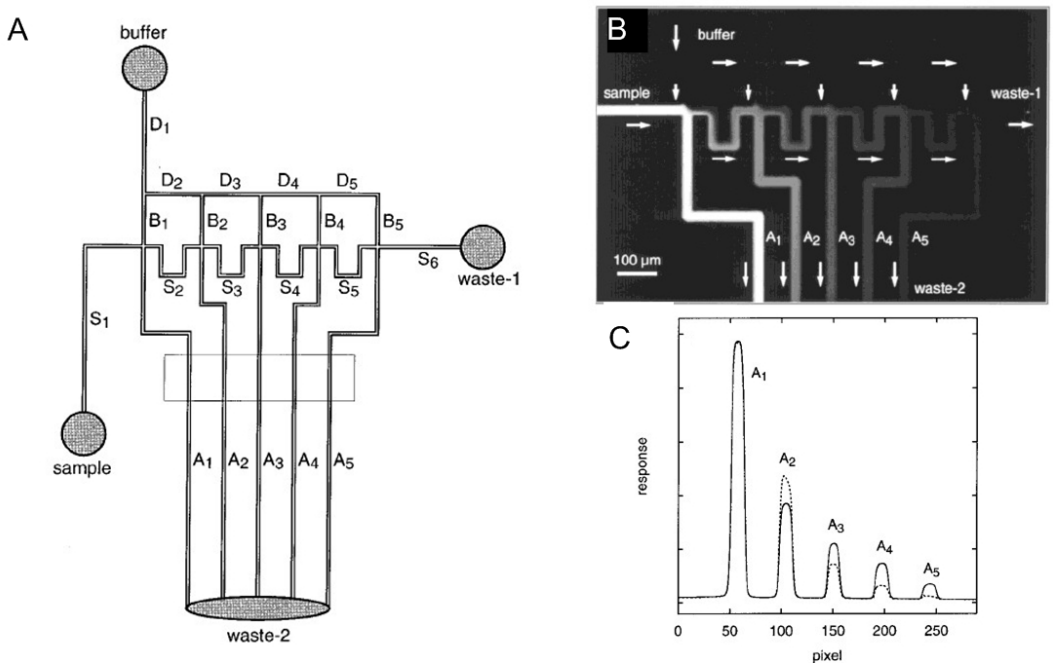

Figure 2.2 (A) Schematic of the microchip for serial electrokinetic mixing, (B) Fluorescent image of the serial mixing of the sample with buffer, (C) Average fluorescent intensity in the microchannels
Source: [(Jacobson, McKnight et al. 1999)]

Seong at al (2003) developed the continuous flow microfluidic system for determination of enzyme kinetics (See Figure 2.3). The left photos in Figure 2.3 are the schematic illustration of the chip (top) and fluorescent micrograph of the microreactor

during continuous flow operation (bottom). The enzyme on microbeads was immobilized into a microreactor and the substrate solution flowed over the reactor from (a) to (b) in Figure 2.3 for performing enzyme reactions. The required samples for conducting enzyme reactions in the chip are 10^9 enzyme molecules and ~ 10 μL of substrate solution.

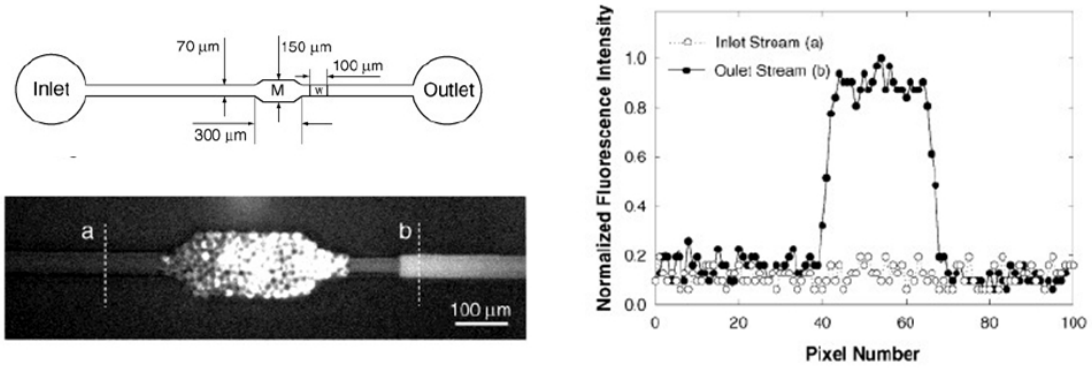

Figure 2.3 Scheme of continuous flow microfluidic system for determination of enzyme kinetics (left) and normalized fluorescence intensity line scans obtained at the locations between (a) and (b) (right)
Source: [(Seong, Heo et al. 2003)]

Burke et al. (2003) developed stopped-flow enzyme assay on a chip using a microfabricated mixer to perform more rapid and efficient mixing than the T mixer that is normally used in continuous flow-based microfluidic assay. Since high mixing efficiency is critical to determine the reaction rate, their system is beneficial for the study of enzymatic reactions.

2.3 Digital microfluidics

Alternatives to the continuous-flow microfluidics are droplet-based microfluidics.

The microfluidic platforms include open structures, where the liquid is divided into controllable droplets, and these droplets can be manipulated to move on a substrate. Numerous methods for manipulating microfluidic droplets have been proposed in the literature (Gallardo et al. 1999; Ichimura et al. 2000; Sammarco and Burns 1999; Jones et al. 2001)**.**

Song et al. (2003) suggested droplet-based microfluidic platform to extract kinetic parameters on millisecond time scale. Their device included rapid on-chip dilution, multiple time range access, compatibility with an enzyme, and explicit treatment of mixing for improving time resolution of the system. They successfully measured single-turnover kinetics of ribonuclease A with better than millisecond resolution using submicroliter volumes of solutions. Figure 2.4 shows the scheme of the design, principles of operation, and measuring single-turnover kinetics of ribonuclease A on the chip.

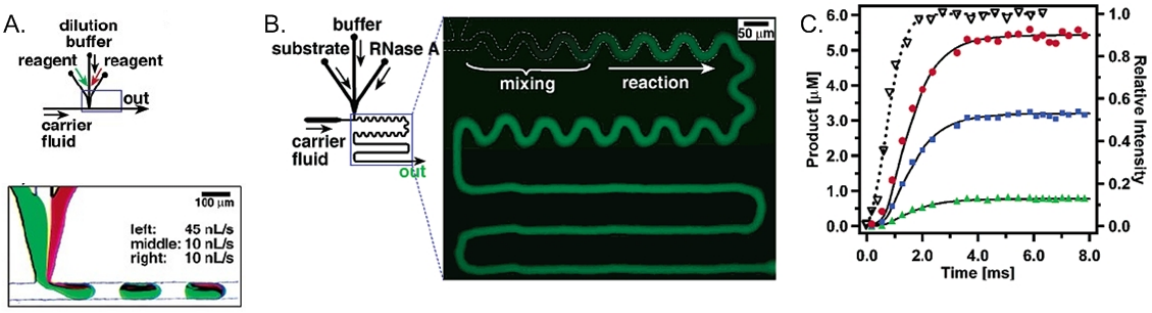

Figure 2.4 Droplet-based microfluidic device for measuring single-turnover kinetics of ribonuclease A (A) On-chip dilution by varying the flow rates of reagents (B) Scheme of the microfluidic platform and a false-color fluorescence microphotograph (C) Reactions progress on a chip
Source: [(Song and Ismagilov 2003)]

2.4 Pneumatically controlled microfluidics

Jambovane et al. (2009) presented an enzyme kinetics chip with 11 parallel reactors. This platform showed the possibility to obtain series of enzyme reactions by using micro metering units and active mixing. The microfluidic device performed 11 enzymatic reactions for the determination of kinetic parameters with a variable parameter in the reactions, the concentration of a substrate.

2.5 Summary

A survey of the literature has shown that much of the research in microfluidics has focused on developing reliable and high-throughput microplatform conducting enzyme reactions on a chip. Some studies suggest microdevice based on microchannel networking by using electrokinetic flow, while other researches introduced droplet-based microfluidic platform for performing rapid reactions on a chip. The alternative to these microchips could be pneumatically controlled microchip.

Since the advantages of microfluidic platform, including reduced consumption of samples and reagents, shorted analysis time, greater sensitivity, and disposability have become more potential for more theoretical plates in engineering, chemistry, and biology, microfluidic platforms are required for biotechnology and medical applications. The simultaneous collection of reaction rate data across a wide range of conditions is easily achievable, making the generation of landscapes to map kinetics behavior of important biological processes an attainable reality.

CHAPTER 3
MICRO ACTIVE MIXER

3.1 Introduction

Robust and reliable mechanical mixing regimes can play important roles in microfluidic and nanofluidic systems, because of the accurate and fast manipulation of liquids in picoliter levels, in addition to almost unlimited sample choices (Chou, Unger et al. 2001; Oddy, Santiago et al. 2001; Stroock, Dertinger et al. 2002; Vilkner, Janasek et al. 2004; Hessel, Lowe et al. 2005; Nguyen and Wu 2005; Huiqian, Nguyen et al. 2006). Here, experimental evaluation of the active micromixers, fabricated by multilayer soft lithography, is studied. Three different mixing loops – circular, triangular, and rectangular – were designed, and their mixing performances were tested according to the position and the width of the valves that drive nanoliters of fluids. Through this research, it was found that a rectangular shape micromixer is better or equal to the ring-shaped microfluidic loop in terms of its mixing efficiency. This study not only provides an improved understanding of the flow behaviors inside the micromixers and design guidelines, but also contributes to the building of higher order complex fluidic systems for complicated biochemical processes on a chip.

3.2 Device design

Each mixer chip with three different mixers also comprises two layers: the top fluidic layer and the bottom control layer. The fluidic layer has flow channels, and the control layer has control channels connected to shutoff valves and mixing valves. Each mixer has eight shutoff valves. Among them, two centerline valves initially close two points of the mixing loop to prevent the contact between the two fluids to be mixed, and are opened when the mixing has started. Another six shutoff valves are initially open while the two fluids are infused into the mixing loop, but are closed during the actual mixing to prevent leakage from the mixing loop. There are three mixing valves in each mixer. By the sequential motion of the valves, fluids in the mixing loop are moved and mixed.

To investigate the effect of the geometry on the mixing performance, this study varied the distance between the mixing valves, mixing valve width and the mixing loop shape. In mixer chips A and B, the distance was varied between the mixing valves by changing the central angle between the mixing valves in the circular mixing loop from 10° to 90° (as shown in Figure 3.1). Figure 3.2 shows that the mixing valve width was varied from 100 ㎛ to 300 ㎛ in mixer chip C. In addition to the circle, a triangle and rectangle were used as mixing loop shapes in mixer chips D and E, as shown in Figure 3.9. For mixer chip E, there is one bending of the flow channel between two mixing valves to study the effect of the bending on the mixing performance.

The typical dimensions of the flow channels are 100 ㎛ in width and 10 ㎛ in height

for all mixer chips. The height of the control channels is 10 ㎛. The width of the control channels is 50 ㎛, except for the valve area. For shutoff valves and mixing valves, the width is typically 200 ㎛, while the mixing valve width is varied in mixer chip C. Overall, when one geometric parameter was changed, other parameters were fixed.

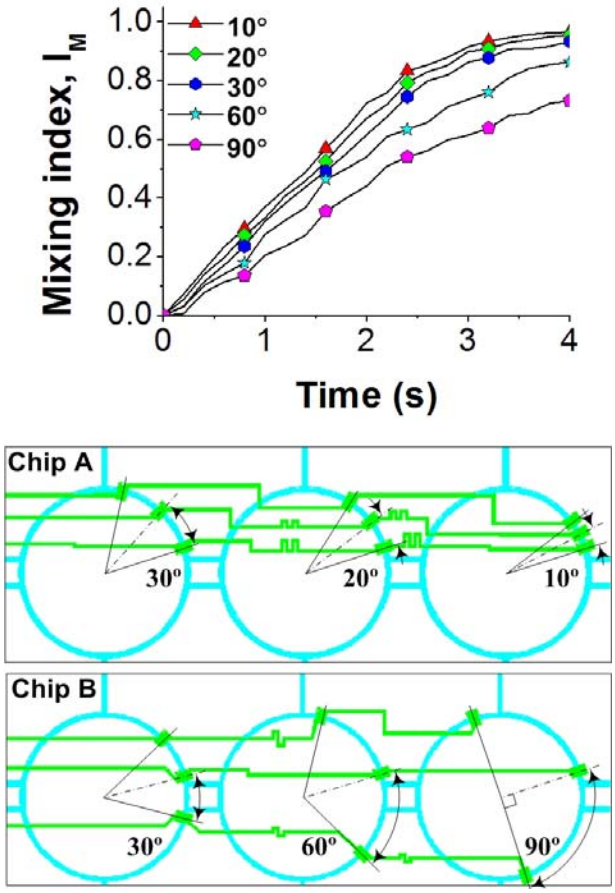

Figure 3.1 Effect of central angle between neighboring mixing valves on mixing performance; the central angle is proportional to the distance between the mixing valves and it is varied from 10° to 90° in chips A and B as shown below (loop shape: circle, mixing valve width: 200㎛).ly controlled microfluidic devices. (a) Simple on-off valve. (b) Peristaltic micropump

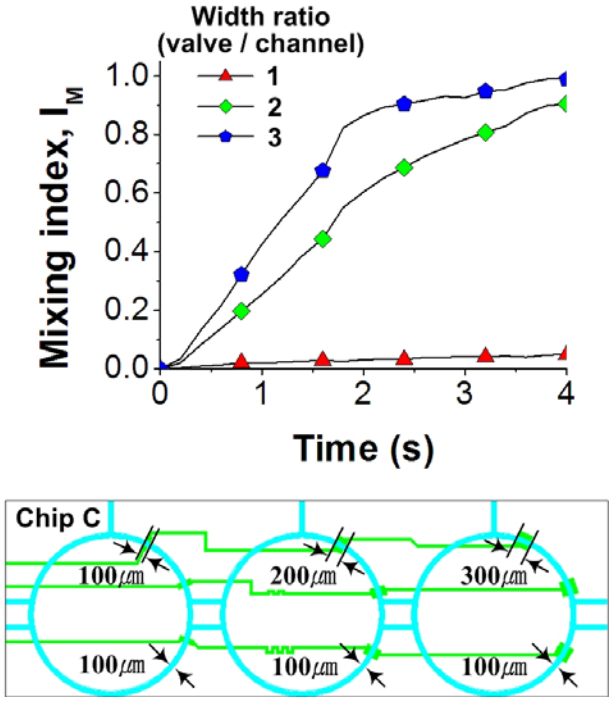

Figure 3.2 Effect of mixing valve width on mixing performance; the mixing valve width is varied from 100㎛ to 300㎛ in chip C as shown below (loop shape: circle, angle between mixing valves: 30°)

3.3 Fabrication

The mixer chips were fabricated by using the multilayer soft lithography technique (See Figure 3.3) (Xia and Whitesides 1998; Unger, Chou et al. 2000). Mask designs were prepared with the AutoCAD software (AutoDesk Inc.) and printed on a transparent film at 20000dpi (CAD/Art Services, Inc.). By using the photoresist-based photolithographic techniques, we fabricated molds for the two layers. At first, positive photoresist (AZ P4620) was spin-coated onto a 4" silicon wafer. This was followed by mask exposure and development. For reliable opening and closing of valves, the cross-sectional shape of flow channels was rounded by heating the mold at 130^{o}C for two

minutes. The top thick fluidic layer of the chip was made by pouring uncured PDMS (GE RTV615; elastomer:cross-linker=10:1) onto the fluidic layer mold to achieve thickness of 5 ㎜. The bottom control layer of the chip was made by spin-coating uncured PDMS (elastomer:cross-linker=20:1) onto the control layer mold at 2800 rpm for one minute. The resultant thickness of the control layer was 29±2 ㎛.

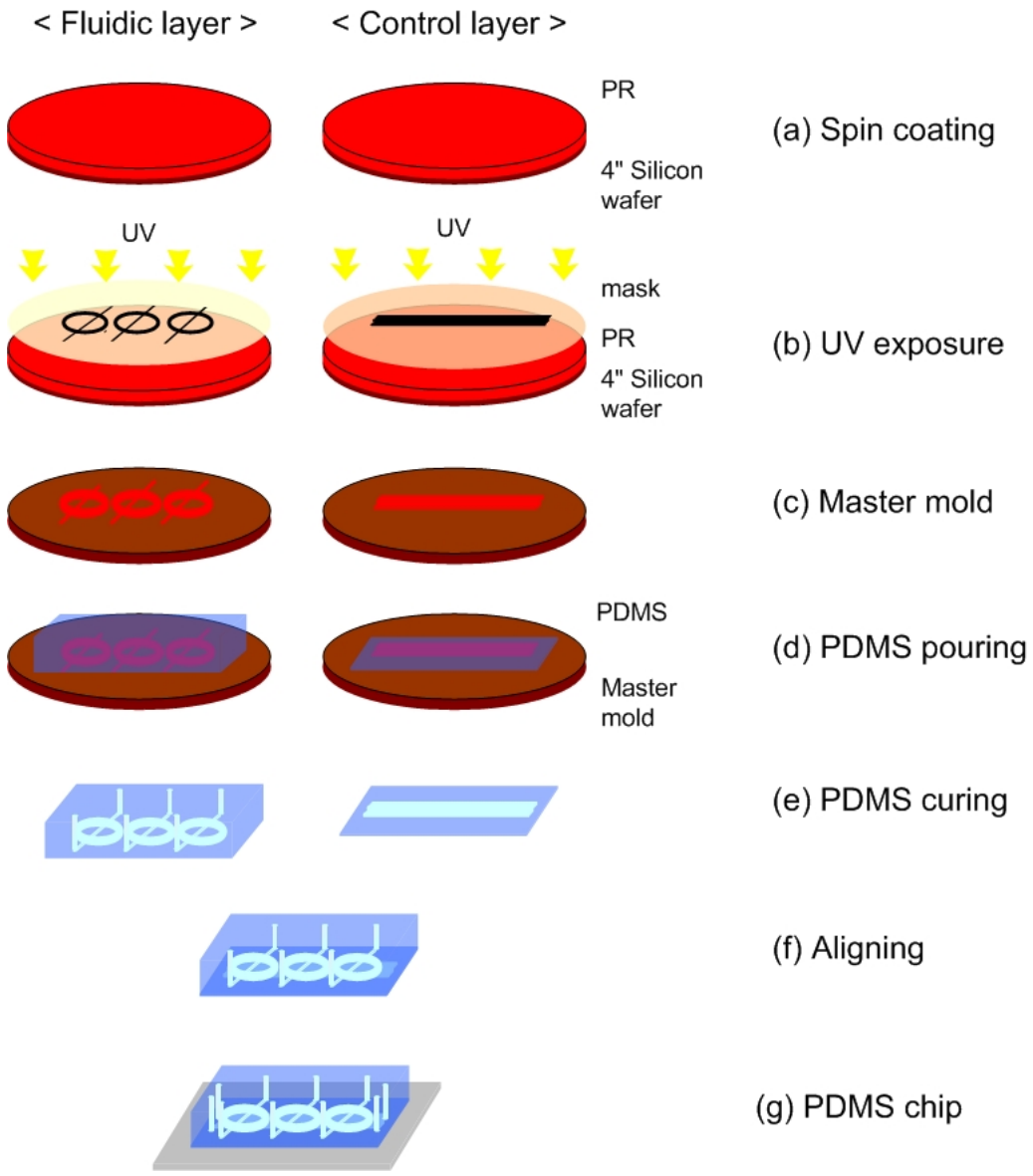

Figure 3.3 Fabrication steps of the mixer chip

The layers were then cured for one hour (fluidic layer) and 45 minutes (control layer) at 80^{o}C. The fluidic layer was peeled off from the mold and holes for input/output ports to flow channels were punched through the thick layer with a 19-gauge punch (Technical Innovations PV-A). After this, the fluidic layer was aligned over the control

layer. The two layers were then bonded by baking them at 80°C for 45 minutes. The bonded layers were peeled off from the control layer mold, and holes for input ports to control channels were punched. Finally, the PDMS chip was covered by a pre-cleaned glass slide (Fisher Science Education PK72) and baked in oven at 80°C for 18 hours to advance adhesion.

3.4 Experimental setup

Figure 3.4 shows the fabricated mixer chip and the experimental setup.

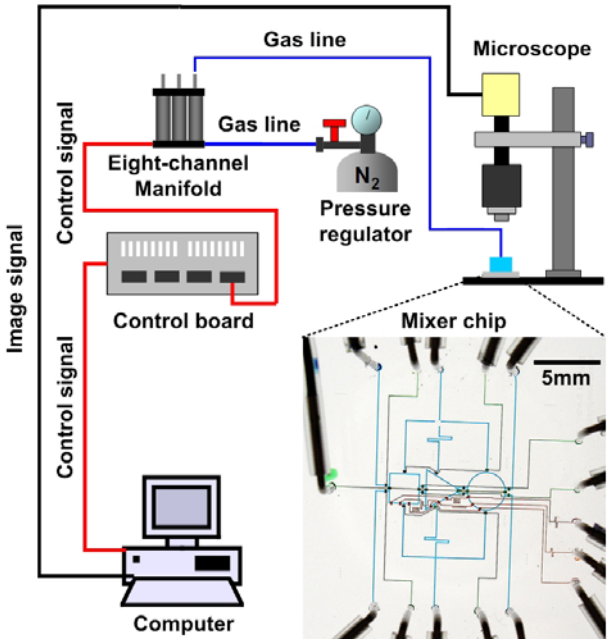

Figure 3.4 Experimental setup and fabricated mixer chip (chip D); all channels of the mixer chip are filled with food dyes (flow channels: blue, control channels connected to shutoff valves: green, control channels connected to mixing valves: red) to show the planar configuration of the fabricated mixer chip

and captured images by using a PC-controlled color digital camera (Motic Moticam 1000). By using Image J software, all captured images were processed to obtain the

average gray value for the mixer area. The mixer chip was operated by pneumatic control. Compressed nitrogen gas was used to pressurize the control channels. Since PDMS is permeable to gases, the tubing connecting the pressure source with the shutoff valves was filled with water to avoid bubble formation inside the flow channels. In contrast, the tubing connecting the pressure source with mixing valves was not filled with water, because the water-filled tubing is not highly sensitive to the applied gas pressure. Since viscosity of water is about 100 times as large as that of nitrogen gas, the water located between the pressure source and the mixing valves can play a role as a dampener for the pressure stimulation. Consequently, when the tubing connecting the pressure source with mixing valves is filled with water, the mixing performance is seriously lowered (as shown in Figure 3.4). In addition, the study found that the gas permeation into the mixing loop was negligible during the experiment. The volume of gas permeation through the PDMS membrane can be calculated as follows:

$$V = \frac{P\Delta pAt}{L}$$

where V, P, Δp, A, t, and L represent the volume of gas permeation, the permeability, the pressure drop across the PDMS membrane, the membrane area, the time duration for the pressure application, and the membrane thickness, respectively. For the tested cases, P, Δp, A, t, and L are 1.838×10^{-15} ㎡/s·Pa, 15psi, 0.04 ㎟, 1/78s, and 20.9 ㎛. From Eq. (2), the study found that the volume of gas permeation was only 4.663pl, which is less than 0.05% of the mixing loop volume. Therefore, the present study maximized the mixing performance by directly pressurizing the mixing valves with nitrogen gas without

concern about the gas permeation. To introduce food dyes (ESCO) into the flow channels quickly (within five seconds), the pressure of 5psi was applied to the backside of the dyes.

The pneumatic control setup consists of three sets of eight-channel manifolds (Fluidigm Corporation) controlled through BOB3 control board (Fluidigm Corporation). A digital I/O card (National Instruments PCI-6533) mounted in computer that digitally controls the switching of each channel of manifolds through the BOB3 control board. The study used a custom-built LabVIEW (National Instruments) program for automatic control of individual valves. For each chip, experiments were conducted three times. From the analysis, the uncertainty was found to be 5.0% at the 95% confidence level.

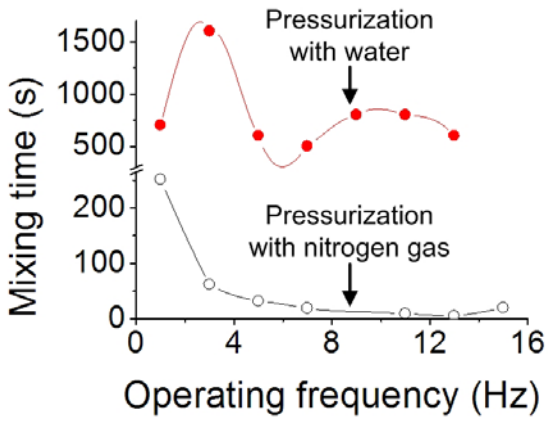

Figure 3.5 Effect of fluid pressurizing mixing valves on mixing performance; when nitrogen gas (hollow circles) is used for pressurizing the mixing valves, the mixing time is dramatically reduced in comparison with the case when water (filled circles) is used (loop shape: circle, angle between mixing valves: 30°, mixing valve width: 200㎛)

3.5 Experiment results

Two food dyes with viscosity almost equivalent to that of water (0.001 Pa·s at 20°C)

were mixed in the peristaltic micromixers to visualize the mixing phenomena, and, based on the captured images, successfully quantified the mixing performance of each mixer. Figure 3.6 shows the captured images on the mixing phenomena that took place inside the micromixer.

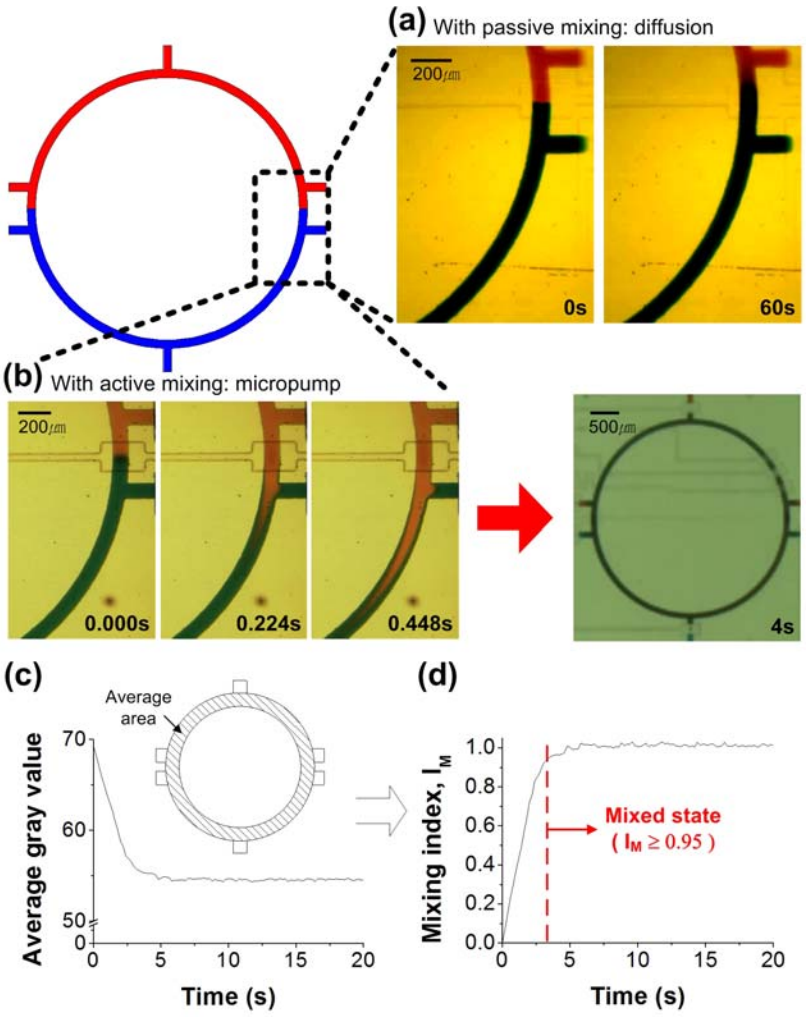

Figure 3.6 Mixing phenomena in mixer chip: (a) mixing by diffusion, boundary layer thickness increases to about 200㎛ in one minute; (b) active mixing by mixing valve operation, mixing is completed within five seconds. (c) quantification of degree of mixing using average gray value for mixer area (hatched region), the average gray value decreases to a steady state value as the mixing progresses; (d) mixing index based on average gray value

When the mixing valves are not working, mixing is dominated by the diffusion and hardly progressed, even within one minute, as explained in Figure 3.6 (a). However, when the mixing valves are working, the interface between the dyes is stretched quickly. Consequently, the mixing is completed within four seconds, as explained in Figure 3.6 (b). To analyze the mixing phenomena quantitatively, in this study, the gray value change during mixing was tracked. Figure 3.6 (c) explains the change of the average gray value of the mixer area for the mixing in Figure 3.6 (b). Figure 3.6 (c) explains that the average gray value is decreased as the degree of mixing is increased. When the mixing is completed, the gray value reaches a steady value. To quantify the degree of mixing based on the average gray value, we define a mixing index as follows:

$$I_M \equiv \frac{G_i - G}{G_i - G_f}$$

where I_M, G_i, G, and G_f represent the mixing index, the average gray values for the initial state, every moment, and the final state, respectively. Figure 3.6 (d) explains the mixing index change for the mixing phenomenon in Figure 3.6 (b). The mixing index is initially zero and increases as the mixing progresses. Finally, when the mixing is completed, the mixing index reaches 1.00. If the mixing time is defined as the time required for the mixing index to reach 0.95, the mixing time for the case explained in Figure 3.6 (b) is 3.6 seconds. This is consistent with what was estimated from the captured images.

The thickness of the membrane between the control channel and the flow channel

was 20.9±2 ㎛. For reliable activation of the membrane, the study applied a pressure of 15psi to the control channels. Under this condition, each mixer was tested for various operating frequency in order to find an optimum value for the operating frequency. Figure 3.7 shows the effects of the operating frequency on the mixing performance.

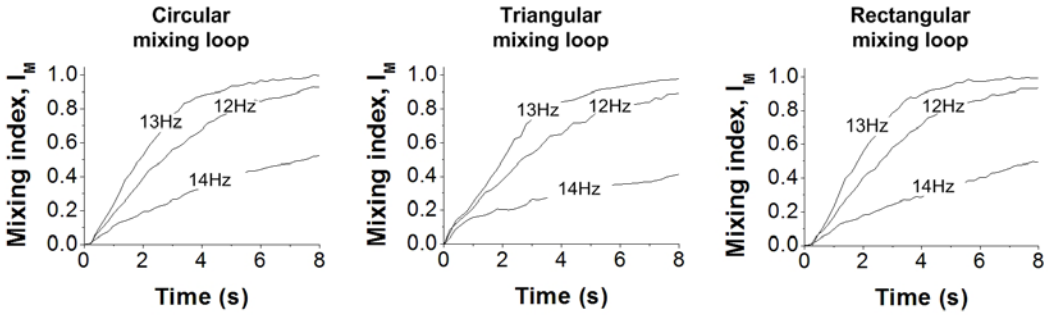

Figure 3.7 Effects of operating frequency on mixing performance; the mixing index increases most rapidly when the operating frequency is 13Hz, regardless of the mixing loop shape

Figure 3.7 shows that 13Hz is best to maximize the mixing performance. Hence, in this study the operating frequency was set to 13Hz in the experimental parametric study.

The smaller the distance (central angle) between the mixing valves, the faster the mixing. When the mixing valve was activated, the pressure around the valve increased and a pressure gradient was developed along the flow channel. Hence, the smaller the distance between the mixing valves, the larger the back pressure for the next mixing valve. This results in more unidirectional flow, yielding faster stretching of the interface between the two fluids. When the central angle is 10°, the distance between the mixing valves is about 76 ㎛. Considering the current level of the microfabrication technology, there is still more room for mixing performance enhancement. In addition to the mixing

performance, decreasing the distance between the mixing valves can lead to more efficient use of space. This is important for highly integrated nanofluidic systems.

Figure 3.2 shows the effect of the mixing valve width on the mixing phenomena, where the valve width was normalized with the flow channel width.

As the mixing valve width was increased, the fluid volume pushed out by the movement of the valve membrane increased. Consequently, flow rate through the mixing loop was increased, which resulted in faster mixing (as shown in Figure 3.2). When the ratio of the mixing valve width to the flow channel width was increased from 1:1 to 1:2 (flow channel width: mixing valve width), the mixing performance was significantly enhanced. However, the degree of enhancement was dramatically decreased as the width ratio increased. Since the design flexibility decreased as the footprint of the valve was increased for a given space in a whole chip design, there would not be apparent merit in increasing the width ratio over 1:3.

Figure 3.8 shows the effects of the mixing loop shape on the mixing of dyes.

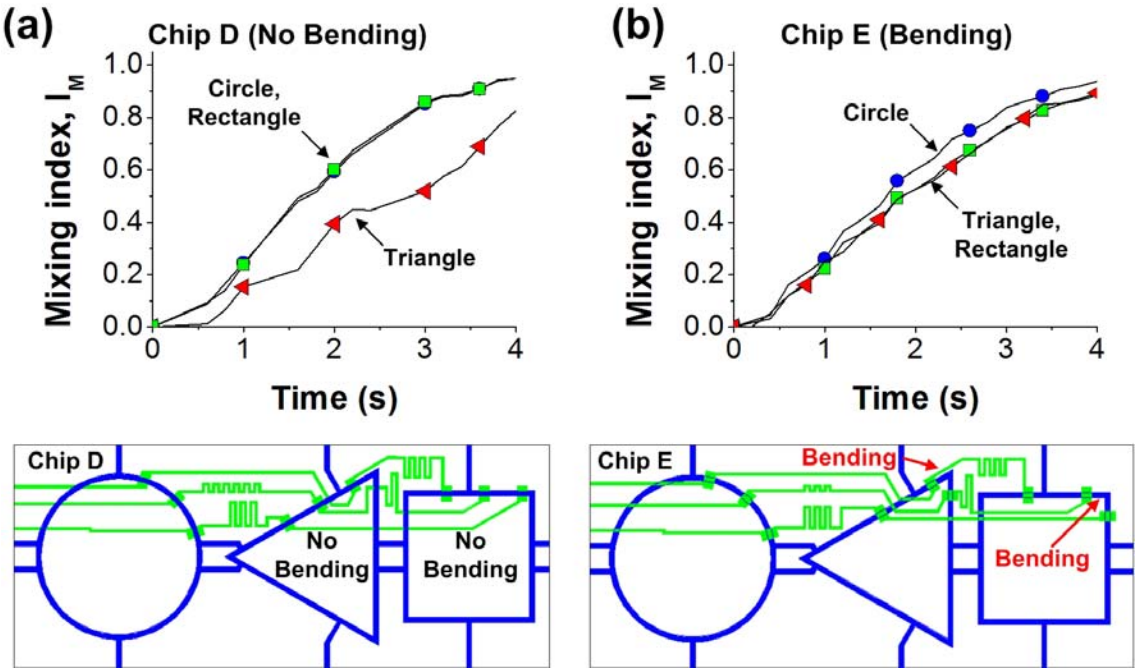

Figure 3.8 Effect of mixing loop shape on mixing performance; the triangle and the rectangle are tested as a mixing loop shape in addition to the circle in chips D and E: (a) mixing index change for mixers without flow channel bending between mixing valves; (b) mixing index change for mixers effect of mixing valve width on mixing performance, the mixing valve width is varied from 100㎛ to 300㎛ in chip (loop shape: circle, angle between mixing valves: 30°)

When there was no flow channel bending between the mixing valves, the rectangular mixer was almost equivalent to the circular mixer in mixing performance, but the triangular mixer was worse than the others (as explained in Figure 3.8 (a)). In contrast, when there was a bending between the mixing valves, the circular shape was best followed by other shapes (as shown in Figure 3.8 (b)). When flow channel bending exists between mixing valves, there are two conflicting parameters influencing the mixing performance. The flow channel bending seriously interrupts the fluid flow between the mixing valves, and these results in deterioration of the peristaltic pumping performance.

This leads to slower stretching of interface between the fluids. In contrast, the flow disturbance due to the bending increases the flow instability, and this improves the mixing in the bending region. For the rectangular shape, the former effect is dominant, and the mixing performance is decreased due to the flow channel bending between the mixing valves. For the triangular mixer, the latter effect is more vigorous, which results in improved mixing.

Overall, the study found that the rectangular mixer without the bending and the circular mixer is the best, and that the flow channel bending between the mixing valves has a positive influence on the mixing performance of the triangular mixer. For the same mixing loop length, the footprint of the rectangular mixer is only 78.5% of that of the circular mixer. In addition, when plural mixing loops are placed on a specified area, the circular shape needs more space around the mixing loop in comparison with the rectangular shape. Therefore, since the rectangular shape is more advantageous than the circular one for large scale integration, it can be concluded that the rectangular mixer is the best choice for highly integrated microfluidic platforms.

All of the experimental results on the effects of the mixer geometry on the mixing time are summarized in Table 3.1.

Table 3.1 Mixing time for peristaltic micromixers

Shape	Angle (°)	Width (㎛)	Bending	Mixing time (s)
Circle	10	200	·	3.6
	20	200	·	3.9
	30	100	·	> 180
		200	·	4.7
		300	·	3.4
	60	200	·	5.4
	90	200	·	7.4
Triangle	30*	200	·	6.8
			O	5.0
Rectangle	30*	200	·	4.2
			O	5.0

* Distance between the mixing valves is equivalent to that of the circular mixer whose central angle between the mixing valves is 30°.

3.6 Conclusions

Except for the mixer with a valve width equal to the flow channel width, the two dyes were mixed within 10 seconds. Based on the experimental parametric study, design guidelines have been derived on the peristaltic micromixer for highly integrated microfluidic platforms as follows:

1. The neighboring mixing valves should be as close as possible.

2. The mixing performance is increased as the mixing valve width is increased, but when both the mixing performance and the design flexibility are considered, it is

good enough for the ratio of the mixing valve width to the flow channel width.

3. Considering both the mixing performance and the space utilization, the rectangular mixer without the flow channel bending between the mixing valves is best for the application of highly integrated microfluidic platforms.

The guidelines listed above would greatly change the layout of the high-throughput integrated nanofluidic systems and improve the overall performance by maximizing the mixing performance of unit mixers.

CHAPTER 4
DEVELOPMENT OF MICROFLUIDIC LANDSCAPER

4.1 Introduction

To investigate the inhibitory catalysis of an enzymatic reaction, conventionally, reagents have been handled using pipettes, flasks or test. Many times, micro-reactors or 96 well plates have been commonly used (Bugg 1997; Hadd, Raymond et al. 1997; Auroux, Iossifidis et al. 2002; Reyes, Iossifidis et al. 2002; Breslauer, Lee et al. 2006). To obtain reliable experimental data, the precise and simultaneous handling of the reactions with multiple reagents is essential. Besides, it is difficult to test different reaction conditions in parallel. In addition, the conventional methods require at least a few milliliters of reagents for a single experiment, and this seriously restricts the inhibitory catalysis evaluation considering the total number of reactions required. To overcome these limitations, exploiting the benefits microfluidic platform, including, efficient handling of multiple reagents, real time gradient generation, small sample size, faster response, and potential of integration into real-time monitoring systems, is required. However, the conventional microfluidic systems, working on continuous flow or droplet based, are unsuitable for multiple and parallel reactions with the requirement of gradient generation reagents.

In this chapter, the microfluidic landscaper system which has a potential to provide powerful microfluidic approach to effectively study the inhibitory pathways involved in the enzyme, substrate, and multi-inhibitor systems was reported. The present system could contribute greatly in understanding enzyme inhibitory kinetics and discovery of new inhibitors/drugs. The great feature of this device is its ability to generate data in three-dimensional landscape, completely novel method of plotting. From this plot, the characterization of inhibitory catalysis could be extremely helpful as the understanding of the inhibitory pathways is vital to predict *in vivo* activities and to discover new multicomponent drugs.

4.2 Device design

4.2.1 Concept of landscaping

For the explanation of the principle of landscaping, it was assumed that the system would have two parameters with three variables each (see Figure 4.1). Based on this, the total number of data points in X-Y plane is nine. Consequently, when a Z value for each X-Y plane data point is given, a landscaped three-dimensional plot can be generated by connecting each data point.

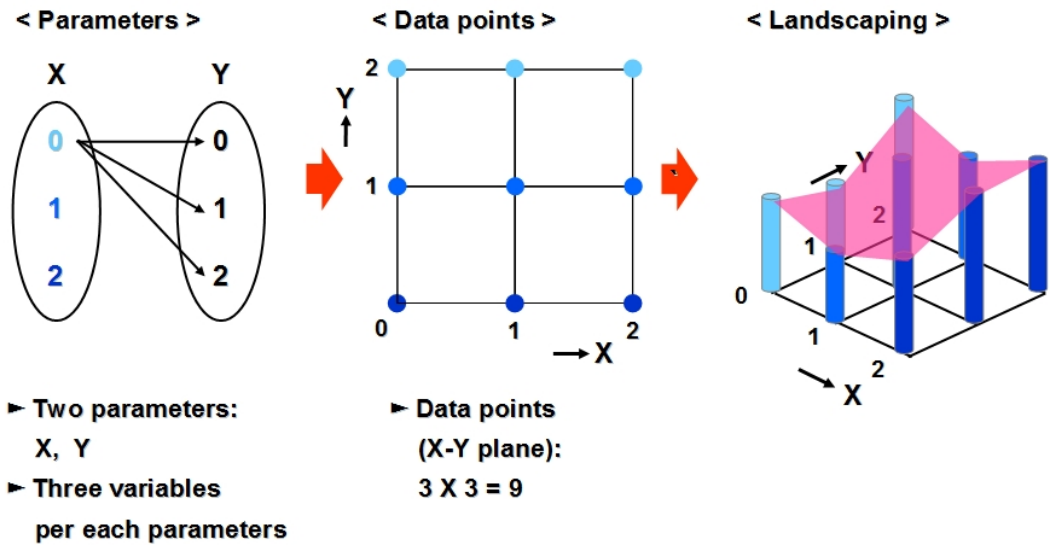

Figure 4.1 Concept of landscaping in principle, with two parameters and three variables per parameter

Using the concept of the landscaping principle, the total number of processors in the microfluidic device was determined. For the device design, two parameters – concentration of substrate and concentration of inhibitor – were selected, since these are the most influential parameters on enzyme reactions. After this, six variables per concentration of a substrate, and seven variables per concentration of an inhibitor, were selected to achieve enzyme kinetic parameters, as well as enzyme inhibitory parameters of the model system. Finally, 42 data points in the X-Y plane were chosen, and three references were added. Figure 4.2 below shows device design, data points, and the landscaping plot. One set of six processors can provide a two-dimensional plot. Consequently, with seven sets of six processors, a landscape variation of reaction rate according to change in concentration of substrate and concentration of inhibitor can be

generated with a single experiment on a chip.

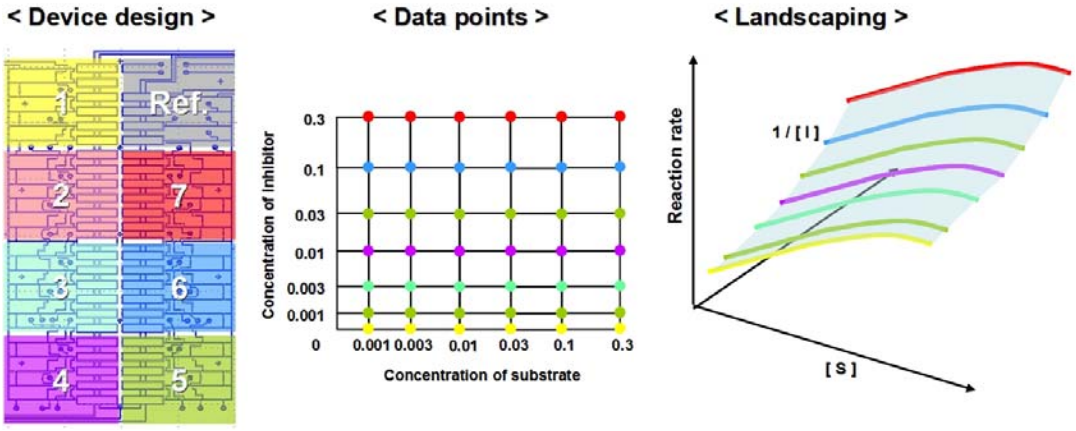

Figure 4.2 Calculation of the number of processors in order to generate landscaping three dimensional plot for the study of enzyme kinetics and enzyme inhibitory kinetics.

4.2.2 Benchmark design scheme 1 (DNA extraction chip)

The concept of automation and integration of experimental procedures, including metering reagents, gradient generation, mixing reagents, and detection, for the protein kinetics was introduced by Hong et al. (2004). They evaluated a highly integrated microfluidic platform for the study of biological and chemical reactions on a chip with parallel processors. However, the number of parallel processors in this device was not enough to adapt enzyme kinetics on a chip.

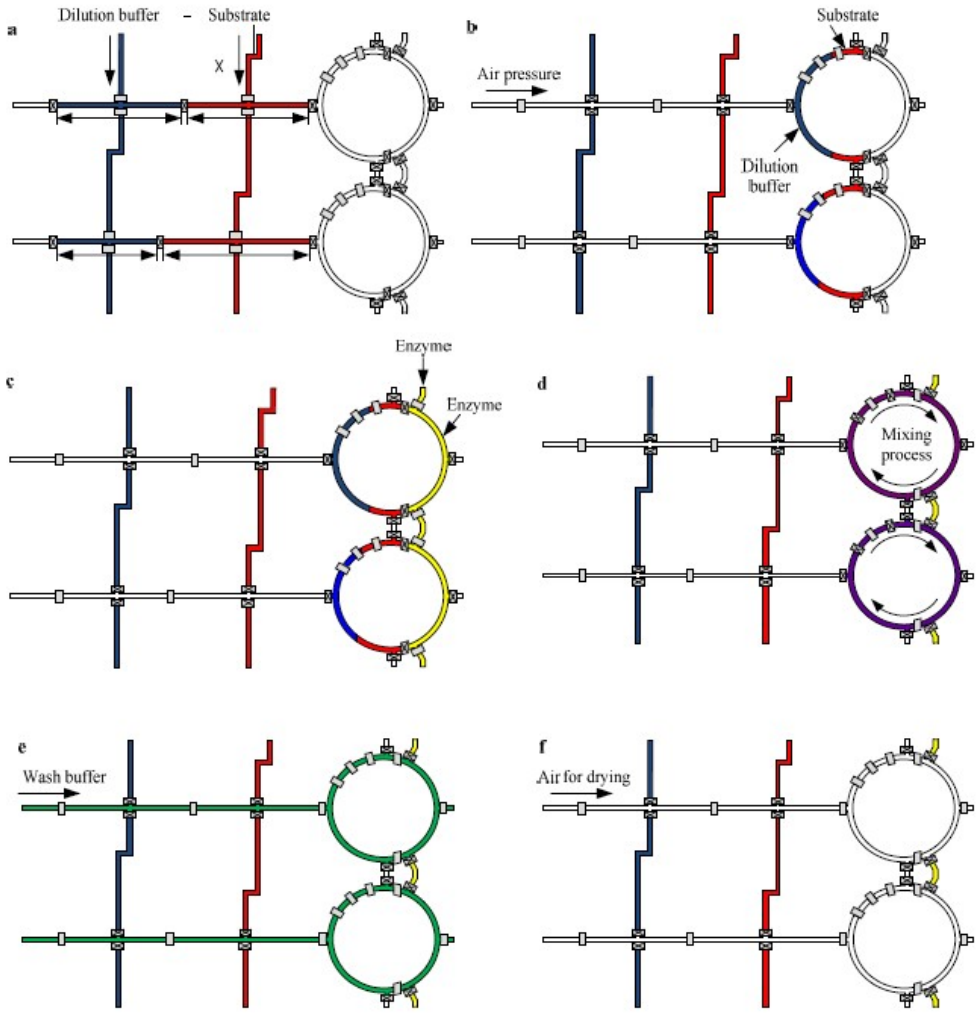

Figure 4.3 Flow of on-chip protein reactions.
Source: [(Hong, Studer et al. 2004)]

4.2.3 Benchmark design scheme 2 (Enzyme kinetic chip)

Jambovane et al. (2009) proposed a fully automated microfluidic platform for determination of enzyme kinetic parameters, with 11 parallel processors. Although the enzyme kinetic chip has great potential to obtain key parameters for enzyme reactions

according to various substrate conditions, it is difficult to show interactions between different substrates. Moreover, the variation in concentrations of substrate in the enzyme kinetic chip, from 1:1 to 1:10, was too short to cover all possible combinations of enzyme reactions within a single experiment.

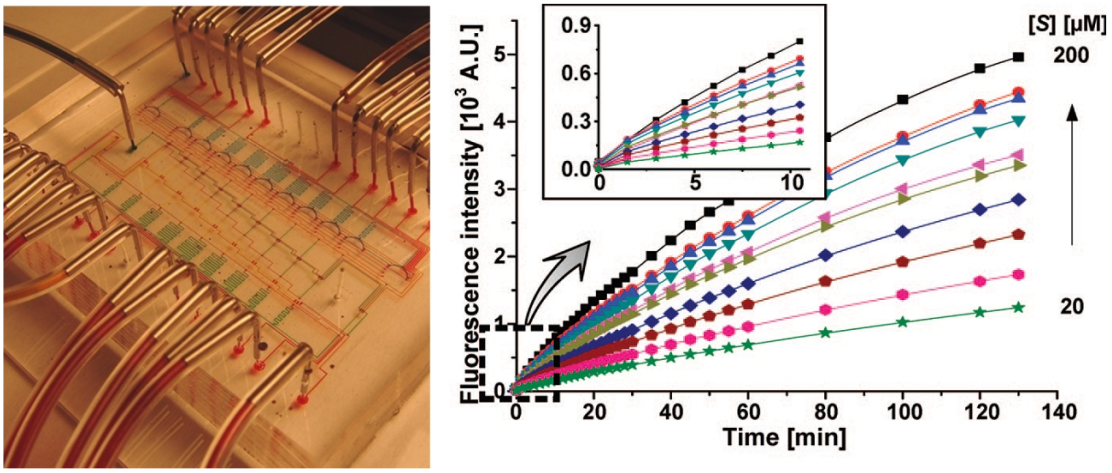

Figure 4.4 The design of enzyme kinetic chip and the results of parallel enzyme reactions performed on the device. The graph shows an increase in fluorescent intensity from the product of the model enzyme reaction according to reaction time, and different lines on the graph represent different concentrations of a substrate. The effect of the substrate concentration in the rate of enzyme-catalyzed reactions was subsequently studied on a chip (Jambovane, Duin et al. 2009)

4.2.4 Microfluidic landscaper version 1.0

The microfluidic landscaper consists of 45 parallel processors to perform enzyme reactions, with 45 combinations of different concentrations of a substrate and an inhibitor for the target enzyme. Series of operation through step-by-step photos are shown as Figure 4.5. With a single experiment on a chip, logarithmic gradients – from 1:1 to 1:1000 –can be accomplished; thereby, fully landscaped information about enzyme inhibitory kinetics as well as enzyme kinetics can be provided in constant conditions,

such as temperature and time. However, the detection range of the scanning system in this study's lab limited monitoring of all enzyme reactions from 1:1 to 1:1000 simultaneously. Since the concentration of reagents in the metering units is determined by the length of metering channels and the initial reagent concentration, the modification of metering units in the device is necessary to detect all reactions on a chip.

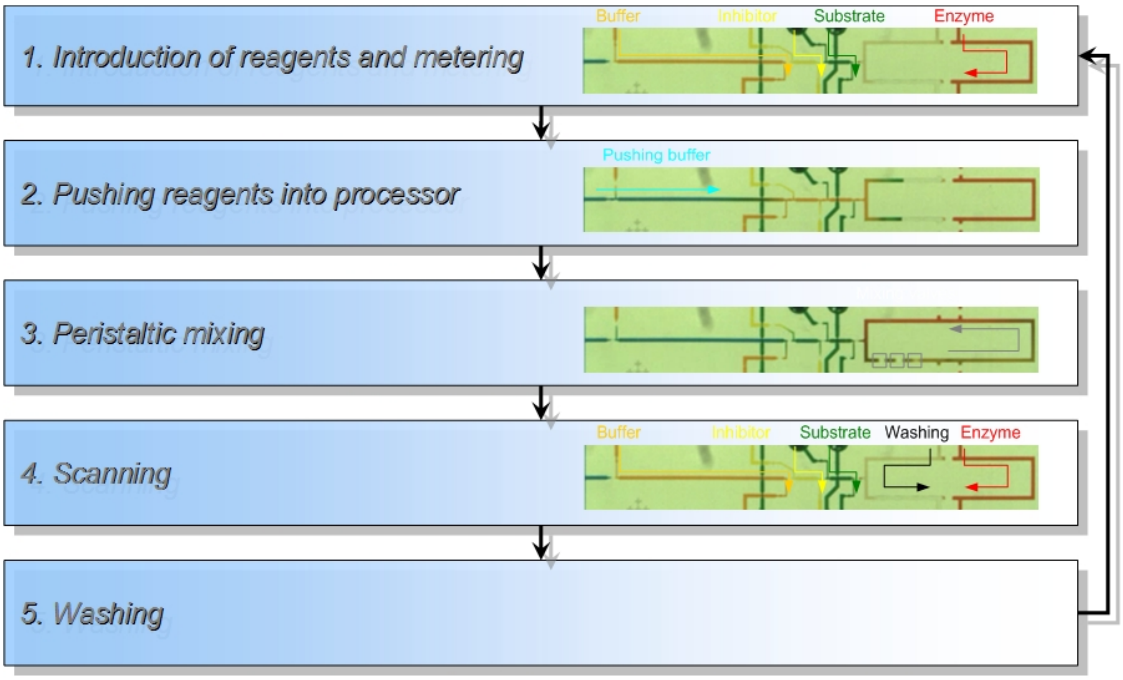

Figure 4.5 Series of operation through step-by-step pictures.
(Note. The real pictures)

4.2.5 Microfluidic landscaper version 2.0

To overcome the detection limit of the scanning system, the metering units in the platform were modified to form a concentration gradient from 1:1 to 1:32. Although the final concentration ranges of reagents in the modified device are narrower than in

microfluidic landscaper version 1.0, the gradients of a substrate and an inhibitor in the device are broad enough to perform enzymatic reactions for determination of enzyme inhibitory kinetic parameters. Figure 4.6 shows AutoCAD design of the whole chip. Green lines, blue lines, and red lines represent upper fluidic channels, main fluidic channels, and control channels, respectively. Figure 4.7 shows two of the 45 processors. The introduction of reagents into the metering channel is achieved through the inlets in this figure. However, while connecting the inlets to the main channels, junctions of fluidic channels were caused. Hence, one more fluidic layer on the main fluidic layer was built up to overcome this challenge. Figure 4.8 shows the different dimensions of the upper fluidic channels and the main fluidic channels. The reagents are loaded the inlets and flow into metering units through main and upper fluidic channels by passing connections between the two fluidic layers. The outlook of a fabricated microfluidic landscaper is shown in Figure 4.9.

Moreover, lowering final concentration ranges of reagents brought more accurate metering. Figure 4.10 shows the comparison of standard curves between previous and modified designs. It was observed that the modified design performed more accurate standard curves, with lower error than in the previous design.

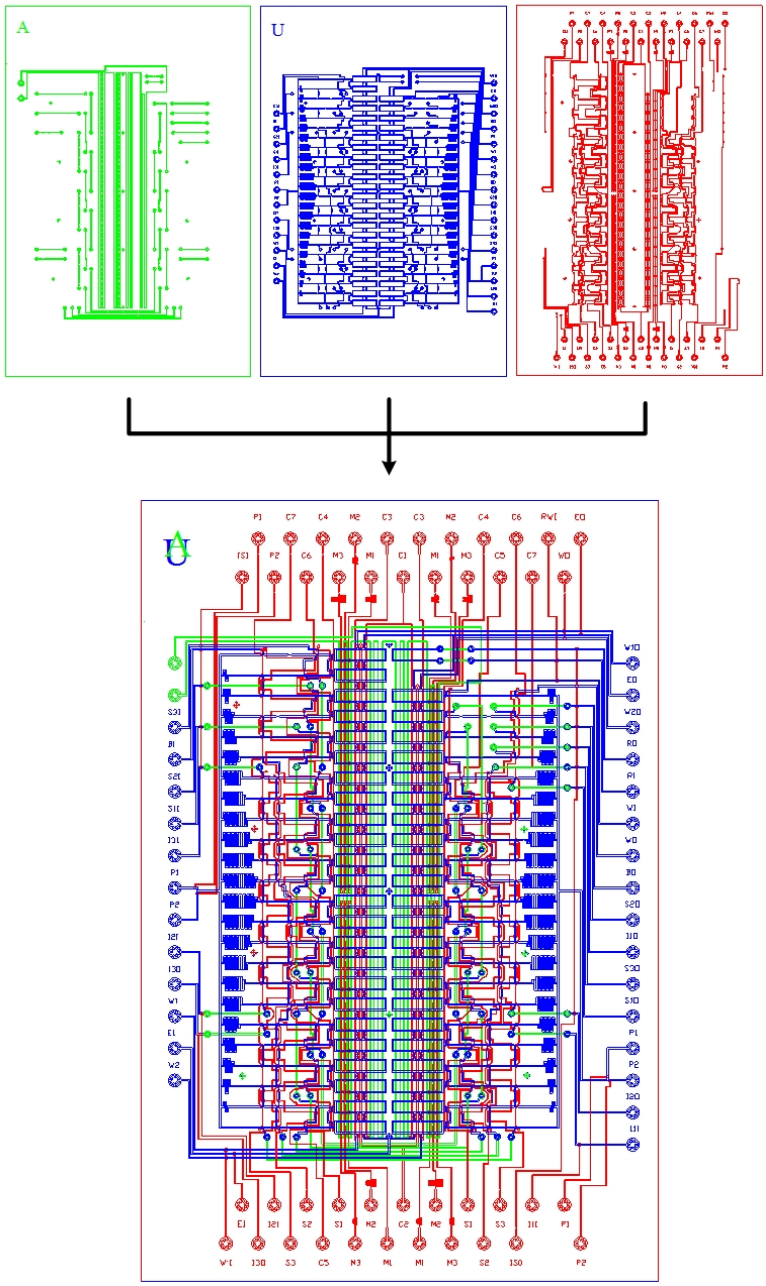

Figure 4.6 AutoCAD design of microfluidic landscaper. The chip consists of three layers, upper fluidic layer (green lines), main fluidic channels (blue lines), and control channels (red lines). The figure on the bottom is the whole design after aligning these three layers.

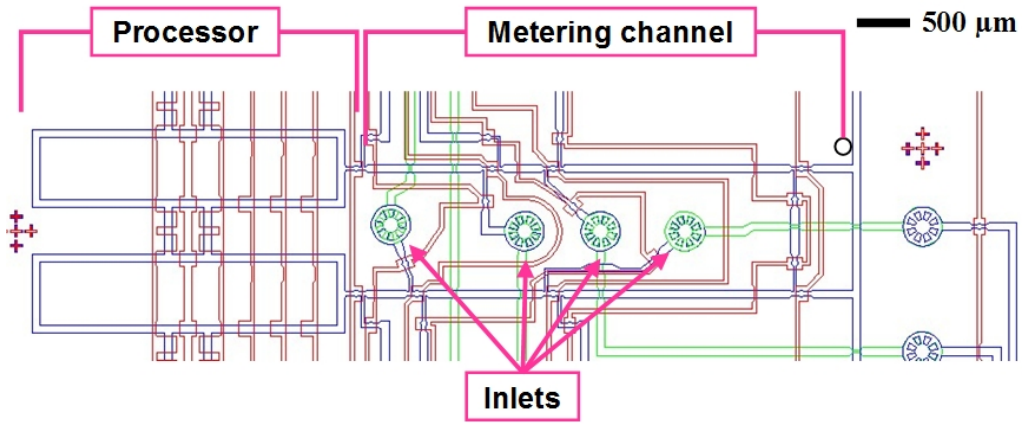

Figure 4.7 Design of the two of 45 processors. Each processor includes its metering unit and three peristaltic mixing valves to complete one reaction.

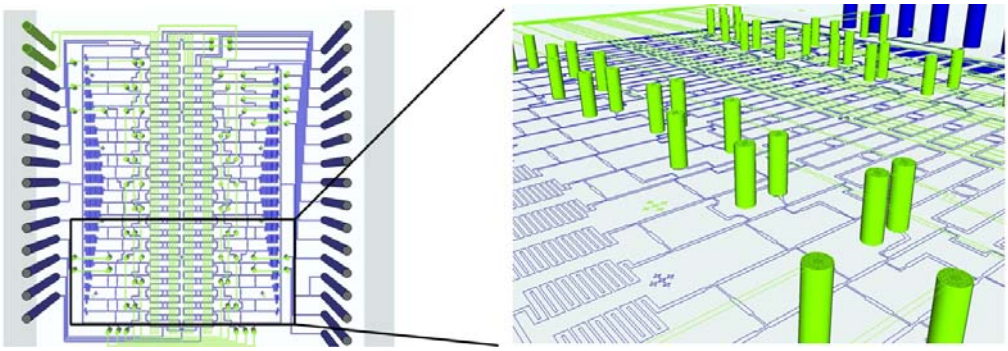

Figure 4.8 Dimensions of the upper fluidic channels (green lines) and the main fluidic channels (blue lines). The channels in the two layers are connected by small holes

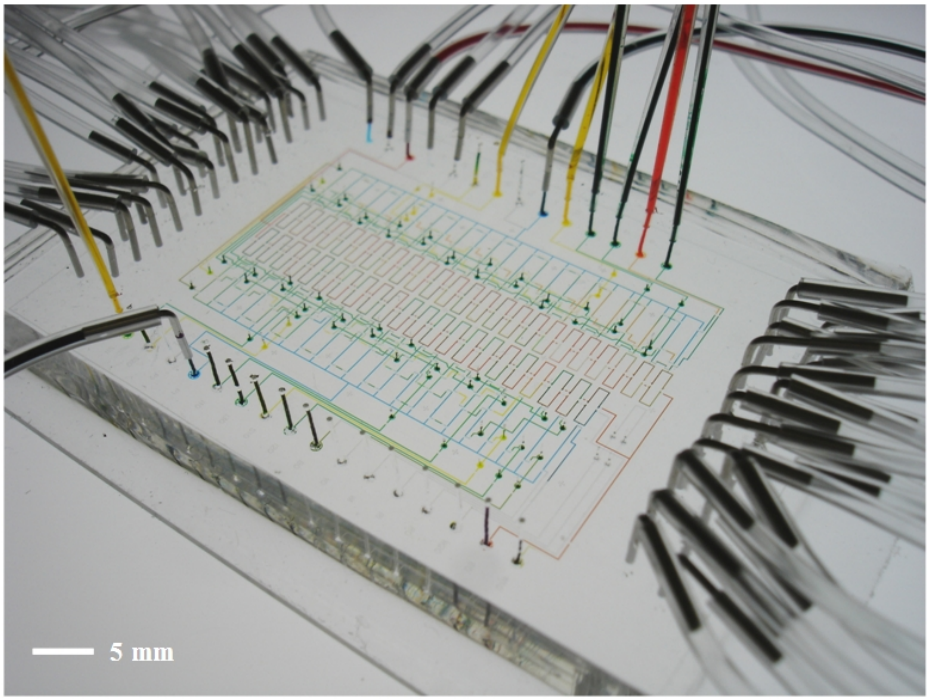

Figure 4.9 Food dye filled microfluidic landscaper

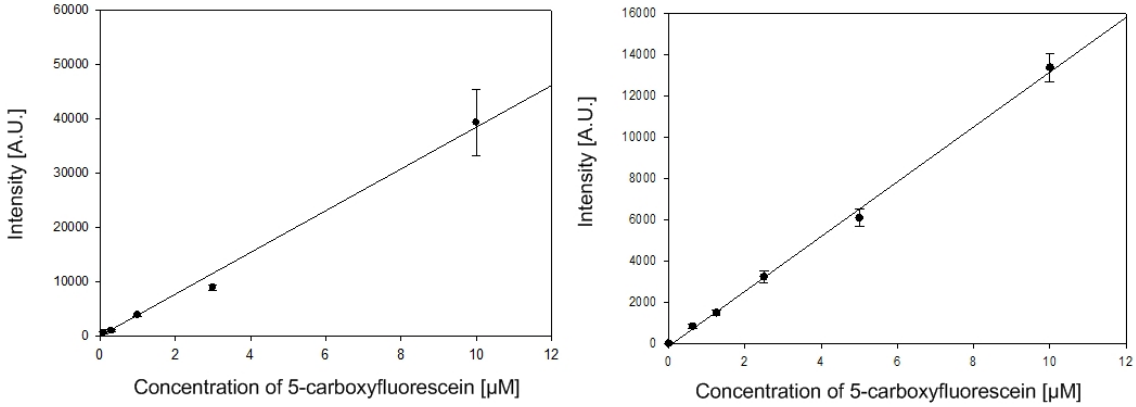

Figure 4.10 Comparison of standard curves between microfluidic landscaper version 1.0 (left) and version 2.0 (right)

4.3 Fabrication

The fabrication steps for microfluidic landscaper are basically same as those of the mixer chip. (See 3.3 Fabrication in chapter 3). However, one more fluidic layer was built up to connect fluidic channels and inlets without junctions of channels. Therefore, the fabrication procedures were modified to obtain the system that has one thick layer and two thin layers. Table 4.1 shows the ratio of polydimethylsiloxane component A to component B and curing time.

Table 4.1 Fabrication conditions of three-layered microfluidic chip

	The ratio of component A to component B	Curing time for the layer	Curing time after aligning layers
Upper fluidic layer	10:1	45 minutes	45 minutes
Main fluidic layer	15:1	30 minutes	
Control layer	20:1	30 minutes	80 minutes

4.4 Device control system

The control systems, including pneumatic control system and observation platform of microfluidic landscaper, are the same as those of the micromixer (see 3.4 Experimental setup).

4.5 Device validation

4.5.1 Mixing efficiency of the device

The geometry of reactors and peristaltic mixing valves was designed based on results

of mixing efficiency in an active micromixer in chapter 3. The guide line from the study shows that a rectangular shaped reactor has higher mixing efficiency than circlular or triangular shaped reactors. Also, the wider mixing valve and the shorter distance between mixing valves are preferred to achieve higher mixing efficiency. Hence, the shape of a reactor in the landscaper was designed as a rectangular shape, and the distance between mixing valves was calculated and designed as short as possible in the outline of the whole chip design.

The operation sequence and pressure were optimized by preliminary experiments with food dyes. Blue food dye was loaded into the halves of reactors, while red dye was loaded into the other halves. The two different food dyes were then mixed through peristaltic mixing by operating mixing valves. Various combinations of sequences in valve operations and pressures for the mixing valves were formed for optimizing the operation conditions. The most stable and highest mixing efficiency was confirmed under the conditions of six step sequences and 18 psi for the mixing valves. Figure 4.11 shows mixing phenomena in a processor with food dyes. The left-hand photos are time series photos of flow generation in a processor by operating mixing valves.

The changes of gray values in 45 processors were captured by using a PC–controlled, color digital camera (Motic Moticam 1000), and processed by using Image J software. Under the optimized operating conditions, 45 reactors achieved more than 95% completed mixing below 15 seconds. The variation in mixing efficiencies of the 45 reactors was lower than 5 % (see Table 4.1).

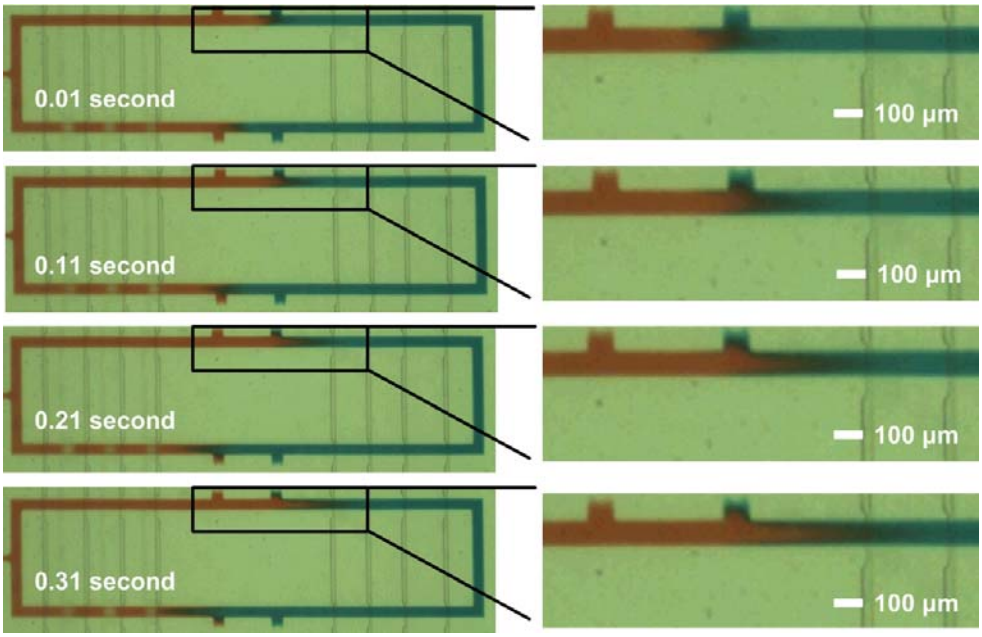

Figure 4.11 Mixing phenomena in a processor

Table 4.2 Mixing time of forty five processors (95 % completed mixing)

Reactor No.	Mixing time (sec)	Reactor No.	Mixing time (sec)	Reactor No.	Mixing time (sec)	Reactor No.	Mixing time (sec)
1	14.4	13	14.4	25	14.4	37	13.8
2	14.3	14	14.5	26	13.9	38	13.9
3	14.9	15	14.5	27	14.3	39	14.1
4	14.9	16	14.5	28	14.4	40	14.2
5	14.9	17	14.5	29	14.2	41	14.2
6	15.1	18	14.2	30	14.1	42	14.2
7	14.6	19	14.4	31	14.7	43	14.4
8	14.6	20	14.5	32	14.8	44	14.9
9	14.6	21	14.4	33	14.6	45	14.3
10	14.5	22	14.4	34	14.8		
11	14.5	23	14.4	35	14.8		
12	14.9	24	14.2	36	14.8		

4.5.2 The accuracy of metering system

To test the functionality of the metering technology, gradients of two different kinds of fluorescent molecules were performed – texas-red (Sigma) and 5-carboxyfluorescein (Anaspec) – on the device. Three different solutions with three different concentrations for each fluorescent molecule were loaded into metering units. The concentrations of loaded texas-red solutions were 62.5 μM, 250 μM, and 1 mM, and 5-carboxyfluorescein solutions were prepared with concentrations of 6.25 μM, 25 μM, and 100 μM. Consequently, the gradient of texas-red covered the concentration range from 25 nM to 400 μM, and the concentration of 5-carboxyfluorescein in its gradient started from 2.5 nM and ended at 40 μM. Figure 4.12 shows the standard curves of texas-red (see Figure 4.12 (a)) and 5-carboxyfluorescein (see Figure 4.12 (b)) within a single experiment.

The texas-red emits fluorescent light at 585 nm with excitation at 530 nm, whereas excitation and emission wavelengths of 5-carboxyfluorescein are 530 nm and 590 nm. Since only one specific molecule in the final mixture of reagents in processors emits fluorescent light at a given wavelength, we can selectively obtain the amount of target molecule in processors by changing the wavelength. This study therefore scanned a device twice at two particular wavelengths – 530 nm and 590 nm – to monitor the amount of texas-red and 5-carboxyfluorescein. In terms of generating gradient for standard curves, six or seven data for one data point can be harvested on a chip; therefore, we can achieve the standard curves with not only gradient of target substrate, but also error range of the specific data point.

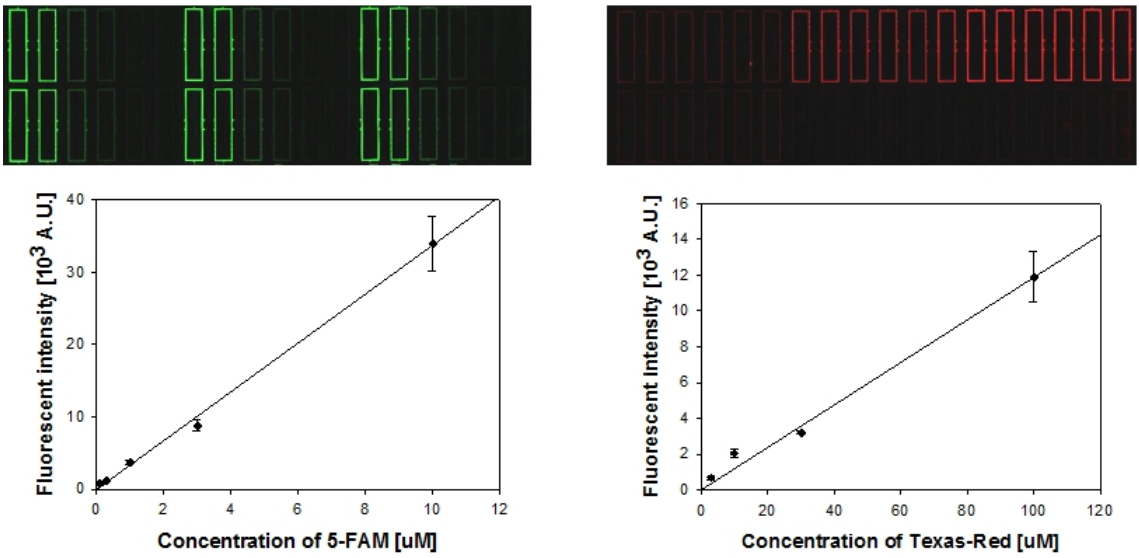

Figure 4.12 Standard curves of the device; two different fluorescent molecules, texas-red and 5-FAM (5-carboxyfluorescein), were loaded into the metering units to check the accuracy of the metering system in the device

4.6 Conclusions

For the purpose of obtaining landscaped enzyme kinetics on a chip, high-throughput microfluidic platform with 45 parallel processors was designed and developed. The fabrication procedures for building up one more layer to the previous two layered microfluidic device were optimized, and the operation system of the device was automated by using LabVIEW. The feasibility of the device was evaluated by performing gradient generation with fluorescent molecules, and mixing phenomena with food dyes as well as a fluorescent molecule.

CHAPTER 5
LANDSCAPING ENZYME BINDING KINETICS ON A CHIP

5.1 Introduction

The feasibility of the successfully developed microfluidic landscaper is confirmed by conducting multiple enzyme-catalyzed reactions with variations of two independent parameters: concentration of a substrate and concentration of an inhibitor. In the study of enzymatic kinetics, not only concentration of reagents, but also the environmental parameters (such as pH and temperature) play key roles (Palmer 1985; Cornish-Bowden 1995; Bugg 1997). However, the experimental conditions, especially environmental temperature, were not precisely optimized; therefore, the results could not follow the ideal enzyme reactions.

5.2 Model enzyme system

5.2.1 Selection of model enzyme system

Basically, there is no specific requirement in the selection of the model enzyme system to conduct its reactions on a chip. The availability of the optical detection system (ArrayWORK® biochip reader) is limited to detect fluorescent intensity within certain ranges. This limitation of this detection automatically sets several guidelines for the

selection of the model enzyme system. Firstly, the model enzyme should be detected through fluorescent intensity, and the intensity according to the progress of the reactions should be higher than the background intensity that could occur during the stitching process of the detection system. Secondly, the reactions should continue for more than five minutes to calculate enzyme kinetic parameters with enough data points. Moreover, the well-known model is preferred for comparing on-chip results to off-chip results from enzyme research groups.

5.2.2 Matrix metalloproteinase-2 enzyme system

Matrix metalloproteinases (MMP-2, 72-kDa gelatinase-A) belong to a family of membrane-associated zinc endopeptidases capable of digesting extracellular matrix components; it is proposed as a therapeutic target for cancer. A series of enzyme reactions with MMP-2 human enzymes was performed to show the ability of this system for the study of enzyme kinetics. 5-FAM/QXLTM520 fluorescence resonance energy transfer (FRET) peptide (AnaSpec) was selected as a target substrate, and Marimastat (Tocris Bioscience) was used as an inhibitor. 5-FAM/QXLTM520 FRET peptide is comprised of 5-FAM (fluorescent molecule) and QXLTM520 (quencher); hence, after its proteolytic cleavage by MMP-2, the fluorescence of 5-FAM is recovered and detected (See Figure 5.1). For the analysis of MMP-2 reactions, this study formed a gradient of 5-FAM-Pro-Leu-OH (AnaSpec) on a chip as a fluorescence reference standard, to obtain the amount of final product of the MMP-2 enzymatic reactions.

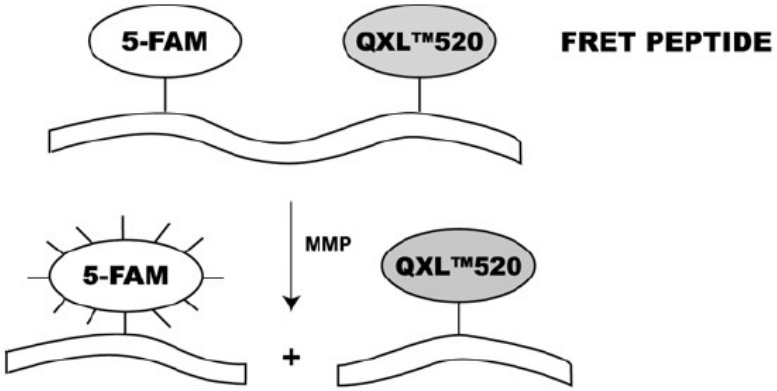

Figure 5.1 Proteolytic cleavage of 5-FAM/QXL™520 FRET peptide by MMPs
Source: [(Anaspec, SensoLyte® 520 MMP - 2 Assay Kit *Fluorimetric*)]

5.3 Material preparations

5-FAM/QXL^{TM}520 fluorescence resonance energy transfer (FRET) peptide, 5-FAM-Pro-Leu-OH reference standard, and matrix metalloproteinase-2 (MMP-2, 72-kDa gelatinase-A, Human) were purchased from Anaspec (Fremont, CA). Marimatstat was obtained from Tocris Bioscience (Ellisville, MO). Dilution buffer solution (50 mM Tris, 10 mM CaCl2, 150 mM NaCl, 0.05% Brij-35, and 0.1% BSA at pH 7.5) was prepared with deionized water from Milli-Q filtration system (Millipore Co.).

5.4 Detection

The microfluidic landscaper was operated by pneumatic control. Compressed nitrogen gas was used to pressurize the control channels (18 psi). To introduce reagents into the fluidic channels, the pressure of 5 psi was applied to the backside of the reagents.

The pneumatic control setup consists of three sets of eight-channel manifolds (Fluidigm Corporation) controlled through BOB3 control board (Fluidigm Corporation). A digital I/O card (National Instruments PCI-6533) mounted in computer that digitally controls the switching of each channel of manifolds through the BOB3 control board. The study used a custom-built LabVIEW (National Instruments) program for automatic control of individual valves. The time-series fluorescent images of the chip were captured by ArrayWORX® biochip reader (Applied Precision®, LLC). The captured images were saved into LINUX®-based computer connected to ArrayWORX® biochip reader.

5.5 Data analysis

The captured fluorescent images by ArrayWORX® biochip reader were processed by using Image J software in order to obtain fluorescent intensity of each image. Then, the change of fluorescent intensity according to time was plotted by Sigmaplot® software, and the enzyme kinetic parameters (K_m and $V_{\max}$), as well as enzyme inhibition kinetic parameter (K_i) were calculated by using Sigmaplot® Enzyme kinetics software.

5.5.1 Standard curves

For the calculation of the amount of products from the detected fluorescent intensity, the standard curve of 5-carboxyfluorescein was performed on the device. Three solutions – 6.25 μM, 25 μM, and 100 μM 5-carboxyfluorescein – were loaded into metering units, whereas the other channels in the metering units were filled with buffer solution (50 mM

Tris, 10 mM CaCl2, 150 mM NaCl, 0.05% Brij-35, and 0.1% BSA at pH 7.5).

Consequently, the final gradient of 5-carboxyfluorescein covered the concentration range from 2.5 μM to 40 μM. After the metering process, the metered reagents were pushed into reactors and mixed by operating three peristaltic mixing valves in a sequence. The intensity of 5-carboxyfluorescein was detected by ArrayWORX® biochip reader at 530 nm / 590 nm (excitation / emission). With single experimentation on a chip, seven fluorescent values for one data point were harvested; therefore, the average fluorescent intensity at a certain concentration of 5-carboxyfluorescein was plotted with its 95% standard derivation. Figure 5.2 shows the relationship between the concentration of 5-carboxyfluorescein and the fluorescent intensity. The increase of fluorescent intensity is directly proportional to the concentration of fluorescent molecules, and the linearity of the curve represents the high metering and mixing efficiency of the device.

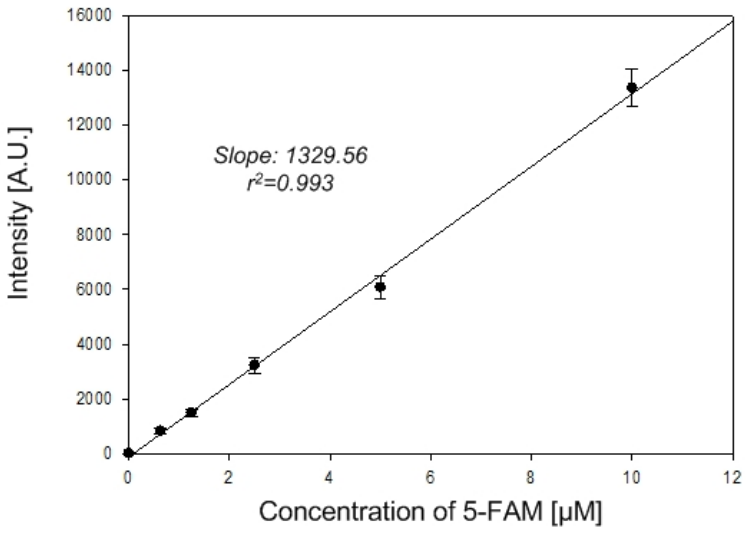

Figure 5.2 Standard curve of 5-carboxyfluorescein

5.5.2 Landscaping MMP-2 enzyme-catalyzed reactions with various concentrations of the enzyme and its substrate

Multiple reactions with various concentrations of matrix metalloproteinase 2 and 5-FAM/QXL^{TM}520 fluorescence resonance energy transfer (FRET) peptide were performed to understanding the relationship between the concentration of the enzyme and the substrate on a chip. 6.25, 25, and 100 μM 5-FAM/QXL^{TM}520 fluorescence resonance energy transfer (FRET) peptide (AnaSpec) and 0.3125, 1.25, and 5 μg/ml matrix metalloproteinase 2 (Anaspec) were prepared and loaded into metering units. The other parts of the chip were filled with reaction buffer solution (50 mM Tris, 10 mM $CaCl_2$, 150 mM NaCl, 0.05% Brij-35, and 0.1% BSA at pH 7.5). After metering process, the reagents in the metering units were pushed into the processors, and mixed by operating

peristaltic mixing valves. The graphs in Figure 5.3 shows increase of fluorescent intensity according to time at a certain concentration of the substrate. Reaction rates with various concentrations of the enzyme, 0.03125, 0.0625, 0.125, 0.25, 0.5 and 1 μg/ml, and various concentrations of the substrate, 0.625, 1.25, 2.5, 5, 10, and 20 μM, were plotted in Figure 5.3. The reaction rate of each reaction that was performed on a chip was calculated by using the mean value of the rate during the first 10 minutes, and plotted with the conditions of the reaction, the concentration of the enzyme and the concentration of the substrate in Figure 5.4. It is shown that rate of enzyme-catalyzed reaction is increased as the concentration of the enzyme or the substrate is increased in Figure 5.4.

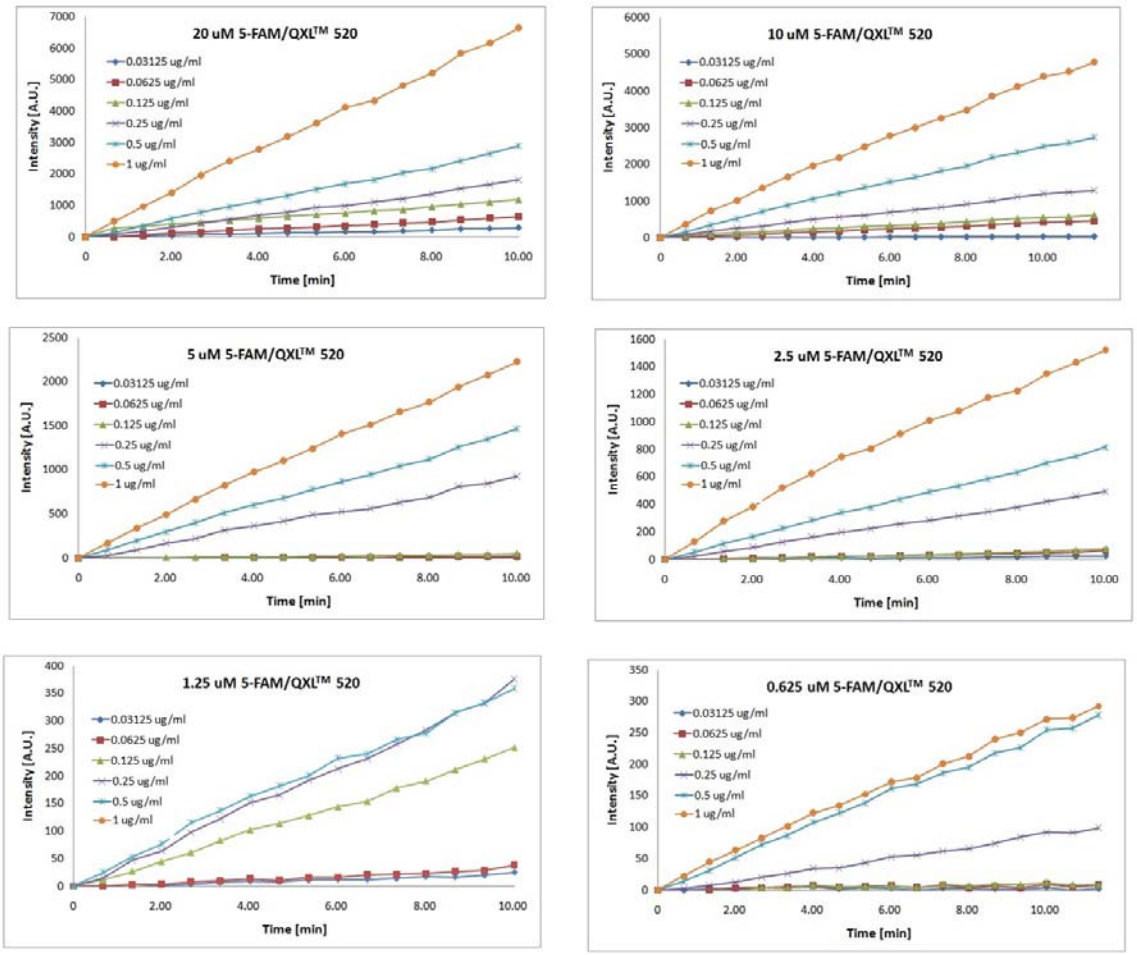

Figure 5.3 Increase of fluorescent intensity according to time at a certain concentration of 5-FAM/QXL^{TM}. Different lines in each graph represent different concentration of matrix metalloproteinase-2.

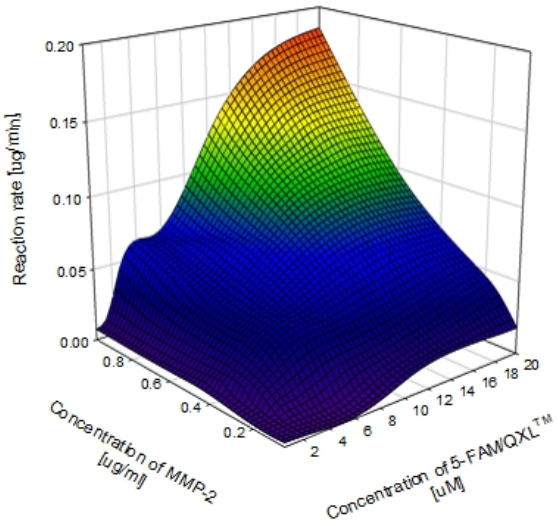

Figure 5.4 Reaction rate with various concentrations of matrix metalloproteinase and 5-FAM/QXL™

5.5.3 Landscaping of MMP-2 enzyme-catalyzed reactions with various concentrations of a substrate and an inhibitor

The study prepared and loaded 6.25 μM, 25 μM, and 100 μM 5-FAM/QXL™520 fluorescence resonance energy transfer (FRET) peptide (AnaSpec) and marimastat (Tocris Bioscience) into metering units. The other parts of the metering units were filled with reaction buffer solution (50 mM Tris, 10 mM $CaCl_2$, 150 mM NaCl, 0.05% Brij-35, and 0.1% BSA at pH 7.5). After metering process, the reagents in the metering units were pushed into the halves of processors, whereas 0.125 μg/ml matrix metalloproteinase-2 solution was loaded into the other halves of processors. Then, reagents in the processors were mixed, and the changes of fluorescent intensity in the processors were monitored by the detection procedure as mentioned in 5.3 Detection. By using above mentioned

procedures, the experiments were repeated three times and the reaction rates were calculated by using Sigmaplot® software. The inhibition of marimastat on matrix metalloproteinase-catalyzed reactions is shown as Figure 5.5.

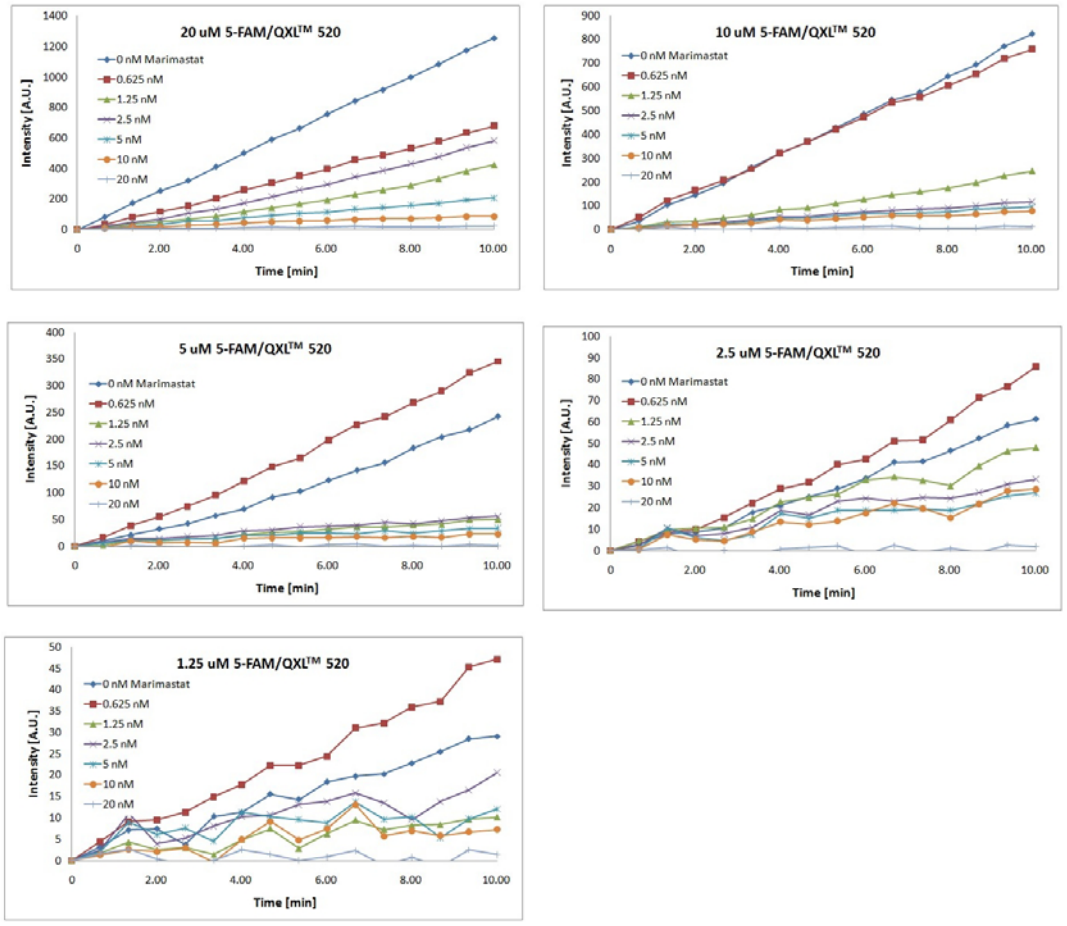

Figure 5.5 Inhibition of marimastat on matrix metalloproteinase-catalyzed reactions

5.6 Results

The concentrations of 5-FAM/QXL™ and marimastat, and the rate of matrix metalloproteinase 2-catalyzed reactions were transferred to Systate Sigmaplot® Enzyme Kinetic module. The curve-fitting of the data was carried out in the same program by using Machaelis-Menten equation. The Machaelis-Menten plot is shown as Figure 5.6.

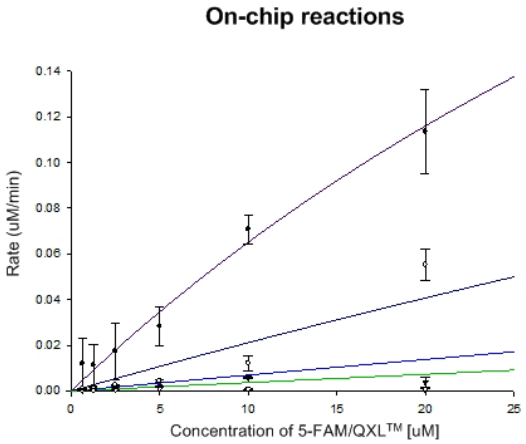

Figure 5.6 Machaelis-Menten plot for matrix metalloproteinase 2

The summary of curve-fitting and kinetic and inhibition kinetic parameters are shown as Table 5.1. The kinetic and inhibition kinetic parameters obtained from microfluidic landscaper were compared to those from conventional experiment in University of Alberta, Canada. (Sariahmetoglu, Crawford et al. 2007)

Table 5.1 Enzyme kinetic and inhibition kinetic parameters for matrix metalloproteinase 2

	Reference (Sariahmetoglu et al. 2007)	**On-chip experiment**
Vmax	38.5 (36.5 to 40.4)	0.5294
Km	33.3 (29.7 to 36.9)	71.3
Ki	N/A	1.1

5.7 Conclusion

Matrix metalloproteinase 2, 5-FAM/QXL^{TM}, and marimastat were selected as the model enzyme, substrate, and inhibitor for conducting multiple enzyme-catalyzed reactions to landscape enzyme kinetics as well as enzyme inhibition kinetics on a chip. Enzyme reactions with variations of two independent parameters: concentration of a substrate and concentration of an inhibitor were automatically performed on a chip, and inhibition of marimastat on the reactions with matrix metalloproteinase 2 and 5-FAM/QXL^{TM} was observed. Comparing on-chip and off-chip results, the on-chip experiment showed higher rates of enzyme-catalyzed reactions than the off-chip experiments. The differences between on-chip and off-chip results could be attributed to the environmental condition: temperature. The temperature of the device varies based on whether it is outside or inside the scanner. Moreover, the real environmental temperature of reactions is different from the surface temperature of the device, since the reaction has occurred inside of the microchannels. The temperature of the device was measured in this study during the detection process, and it reflected an optimization of operation

conditions in the off-chip experiment. However, the measured temperature was the surface temperature of the chip; therefore, there could be differences between environmental temperature of reactions and measured temperature. For the precise control of temperature during performing reactions on a chip, temperature-controlling system, for example Indium Tin Oxide (ITO) heater (Chua, Thornton et al. 1997), could be integrated into the microfluidic landscaper.

5.8 Scientific issues

The microfluidic landscaper was designed and developed to conduct 45 reactions according to different concentrations of two independent parameters at constant concentration of an enzyme. By performing 45 parallel reactions on a microfluidic landscaper, this study showed the effects of an inhibitor on the reactions with an enzyme and its substrate on the chip.

The results of enzyme-catalyzed reactions that were accomplished on a chip show that it is possible to generate multiple biological or biochemical reactions on a chip. To confirm the feasibility of the device, 45 reactions with specific concentration of an enzyme and various concentrations of a substrate as well as an inhibitor were perform for the study of enzyme inhibitory kinetics. When we load another substrate instead of an inhibitor, 45 enzymatic reactions with various concentrations of two substrates at certain concentration of an enzyme could be conducted on a chip. This model system could be used for the application of dug-drug interaction that plays great important role in pharmaceuticals. The study of allosteric regulatory enzymes is also possible on this

device by loading various concentrations of two enzymes and their substrate.

CHAPTER 6
SUMMARY AND CONCLUSIONS

6.1 Conclusions of the research

A new microfluidic system that has a potential to provide with landscaped information about enzyme kinetics and enzyme inhibitory kinetics has been developed. The system consists of forty-five parallel processors to perform enzyme reactions with forty-five combinations of an enzyme and different concentrations of its substrate and inhibitor. With a single experiment on a chip, gradients, from 1:1 to 1:32, in the concentration of a substrate and an inhibitor were accomplished, thereby fully landscaped information about enzyme inhibitory kinetics in matrix metalloproteinase 2 can be provided The results of this research suggest that this automated microfluidic landscaper makes it possible to achieve the catalytic performances of matrix metalloproteinase 2 as a series of three-dimensional landscapes where kinetic parameters plotted as a function of variable concentrations of a substrate and an inhibitor; hence, this system would provide a total view of interactions between a substrate and an inhibitor in matrix metalloproteinase 2 enzyme-catalyzed reactions with a complete understanding of the factors that have an effect on it and the indispensable information needed to obtain the constants governing their influences

REFERENCES

Auroux, P., D. Iossifidis, et al. (2002). "Micro total analysis systems. 2. Analytical standard operations and applications." Anal. Chem 74(12): 2637-2652.

Breslauer, D., P. Lee, et al. (2006). "Microfluidics-based systems biology." Molecular BioSystems 2(2): 97-112.

Bugg, T. (1997). An introduction to enzyme and coenzyme chemistry, Wiley-Blackwell.

Chou, H., M. Unger, et al. (2001). "A microfabricated rotary pump." Biomedical Microdevices 3(4): 323-330.

Chua, C., R. Thornton, et al. (1997). "Indium tin oxide transparent electrodes for broad-area top-emitting vertical-cavity lasers fabricated using a single lithography step." IEEE Photonics Technology Letters 9(5): 551-553.

Cornish-Bowden, A. (1995). Analysis of enzyme kinetic data, Oxford University Press, USA.

Craighead, H. (2006). "Future lab-on-a-chip technologies for interrogating individual molecules." Nature 442(7101): 387-393.

Daw, R. and J. Finkelstein (2006). "Lab on a chip." Nature 442(7101): 367.

Duffy, D., H. Gillis, et al. (1999). "Microfabricated centrifugal microfluidic systems: characterization and multiple enzymatic assays." Anal. Chem 71(20): 4669-4678.

Emrich, C., H. Tian, et al. (2002). "Microfabricated 384-lane capillary array electrophoresis bioanalyzer for ultrahigh-throughput genetic analysis." Anal. Chem 74(19): 5076-5083.

Hadd, A., S. Jacobson, et al. (1999). "Microfluidic assays of acetylcholinesterase inhibitors." Anal. Chem 71(22): 5206-5212.

Hadd, A., D. Raymond, et al. (1997). "Microchip device for performing enzyme assays." Anal. Chem 69(17): 3407-3412.

Hessel, V., H. Lowe, et al. (2005). "Micromixers--a review on passive and active mixing principles." Chemical Engineering Science 60(8-9): 2479-2501.

Hong, J., V. Studer, et al. (2004). "A nanoliter-scale nucleic acid processor with parallel architecture." Nature biotechnology 22(4): 435-439.

Hruby, J. (2001). "Liga Technologies." MRS BULLETIN: 337.

Huiqian, Y., N. Nguyen, et al. (2006). Micromixer based on Taylor dispersion, Institute of Physics Publishing.

Jacobson, S., T. McKnight, et al. (1999). "Microfluidic devices for electrokinetically driven parallel and serial mixing." Anal. Chem 71(20): 4455-4459.

Jambovane, S., E. Duin, et al. (2009). "Determination of Kinetic Parameters, Km and kcat, with a Single Experiment on a Chip." Analytical chemistry 81(9): 3239-3245.

McDonald, J., D. Duffy, et al. (1999). "Fabrication of microfluidic systems in poly (dimethylsiloxane)." Electrophoresis 21(1): 27-40.

Nguyen, N. and S. Wereley (2002). Fundamentals and applications of microfluidics, Artech House Publishers.

Nguyen, N. and Z. Wu (2005). "Micromixers--a review." J. Micromech. Microeng 15(2): R1-R16.

Oddy, M., J. Santiago, et al. (2001). "Electrokinetic instability micromixing." Anal. Chem 73(24): 5822-5832.

Palmer, T. (1985). Understanding enzymes, Horwood.

Reyes, D., D. Iossifidis, et al. (2002). "Micro total analysis systems. 1. Introduction, theory, and technology." ANALYTICAL CHEMISTRY-WASHINGTON DC- 74(12): 2623-2636.

Sariahmetoglu, M., B. Crawford, et al. (2007). "Regulation of matrix metalloproteinase-2 (MMP-2) activity by phosphorylation." The FASEB Journal 21(10): 2486.

Seong, G., J. Heo, et al. (2003). "Measurement of enzyme kinetics using a continuous-flow microfluidic system." Anal. Chem 75(13): 3161-3167.

Song, H. and R. Ismagilov (2003). "Millisecond kinetics on a microfluidic chip using nanoliters of reagents." J. Am. Chem. Soc 125(47): 14613-14619.

Stroock, A., S. Dertinger, et al. (2002). "Chaotic mixer for microchannels." Science 295(5555): 647.

Unger, M., H. Chou, et al. (2000). "Monolithic microfabricated valves and pumps by multilayer soft lithography." Science 288(5463): 113.

Vilkner, T., D. Janasek, et al. (2004). "Micro total analysis systems. Recent developments." ANALYTICAL CHEMISTRY-WASHINGTON DC- 76: 3373-3386.

Whitesides, G. (2006). "The origins and the future of microfluidics." Nature 442(7101): 368-373.

Xia, Y. and G. Whitesides (1998). "Soft lithography." Annual Review of Materials Science 28(1): 153-184.

APPENDIX-A

PREPARATION OF REAGENTS

Reaction buffer solution

50 mM Tris, 10 mM CaCl2, 150 mM NaCl, 0.05% Brij-35, and 0.1% BSA at pH 7.5

Standard fluorescent molecule solution (Texas-red, Sigma)

	Stock solution	Reaction buffer solution	Final concentration
Mixture 1	10 µL 10 mM Texas-red	90 µL	1 mM Texas-red
Mixture 2	25 µL 1 mM Texas-red	75 µL	250 µM Texas-red
Mixture 3	25 µL 250 µM Texas-red	75 µL	62.5 µM Texas-red

Standard fluorescent molecule solution (5-carboxyfluorescein, Anaspec)

	Stock solution	Reaction buffer solution	Final concentration
Mixture 1	10 µL 1 mM 5-FAM	90 µL	100 µM 5-FAM
Mixture 2	25 µL 100 µM 5-FAM	75 µL	25 µM 5-FAM
Mixture 3	25 µL 25 µM 5-FAM	75 µL	6.25 µM 5-FAM

Enzyme solution (Matrix metalloproteinase-2, Anaspec)

	Stock solution	Reaction buffer solution	Final concentration
Mixture 1	20 µL 10 µg/ml MMP-2	20 µL	5 µg/ml MMP-2
Mixture 2	25 µL 5 µg/ml MMP-2	75 µL	1.25 µg/ml MMP-2
Mixture 3	25 µL 1.25 µg/ml MMP-2	75 µL	0.3125 µg/ml MMP-2

Suibstrate solution (5-FAM/QXL^{TM}520 FRET peptide, AnaSpec)

	Stock solution	Reaction buffer solution	Final concentration
Mixture 1	10 µL 1 mM 5-FAM/QXL^{TM}520	90 µL	100 µM 5-FAM/QXL^{TM}520
Mixture 2	25 µL 100 µM 5-FAM/QXL^{TM}520	75 µL	25 µM 5-FAM/QXL^{TM}520
Mixture 3	25 µL 25 µM 5-FAM/QXL^{TM}520	75 µL	6.25 µM 5-FAM/QXL^{TM}520

Inhibitor solution (Marimastat, Tocris Bioscience)

	Stock solution	Reaction buffer solution	Final concentration
Mixture 1	10 µL 1 mM Marimastat	90 µL	100 µM Marimastat
Mixture 2	25 µL 100 µM Marimastat	75 µL	25 µM Marimastat
Mixture 3	25 µL 25 µM Marimastat	75 µL	6.25 µM Marimastat

APPENDIX-B

DATA ANALYSIS

Figure: Fluorescent images obtained by time-series scanning

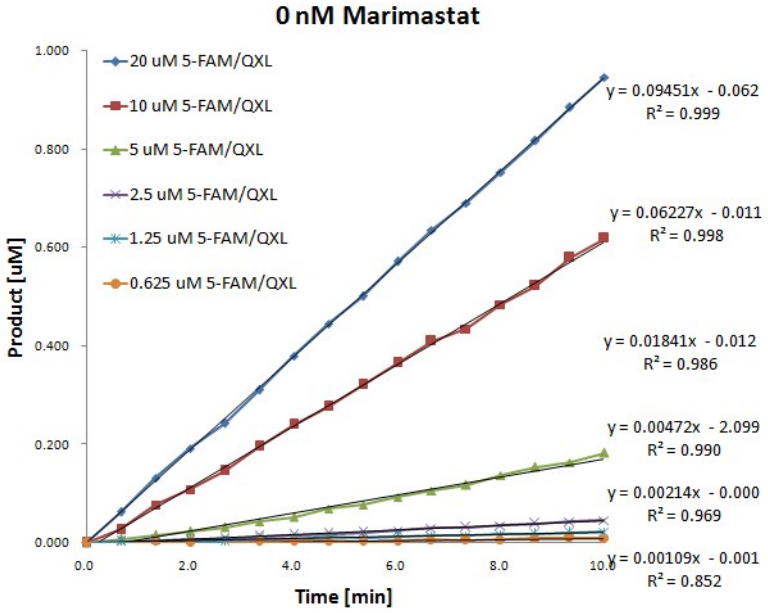

Figure: Velocities for MMP-2 enzyme kinetics experiments

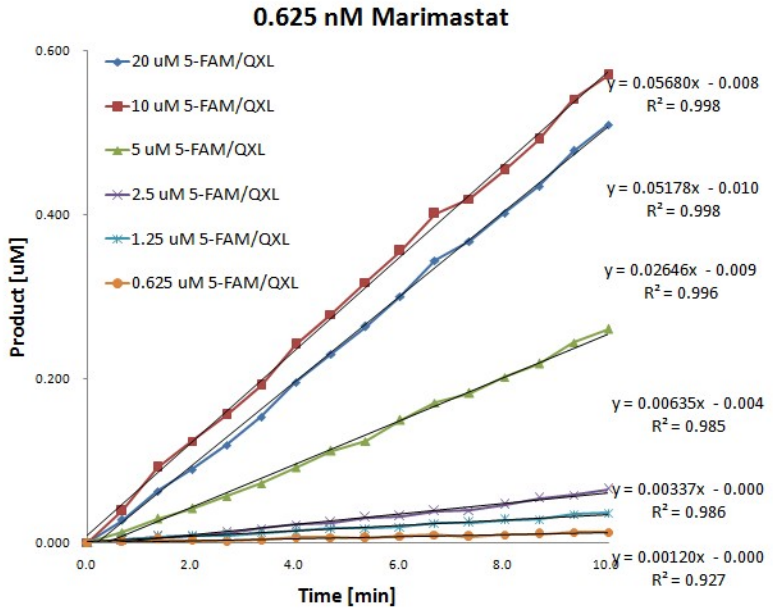

Figure: Velocities for MMP-2 enzyme kinetics experiments

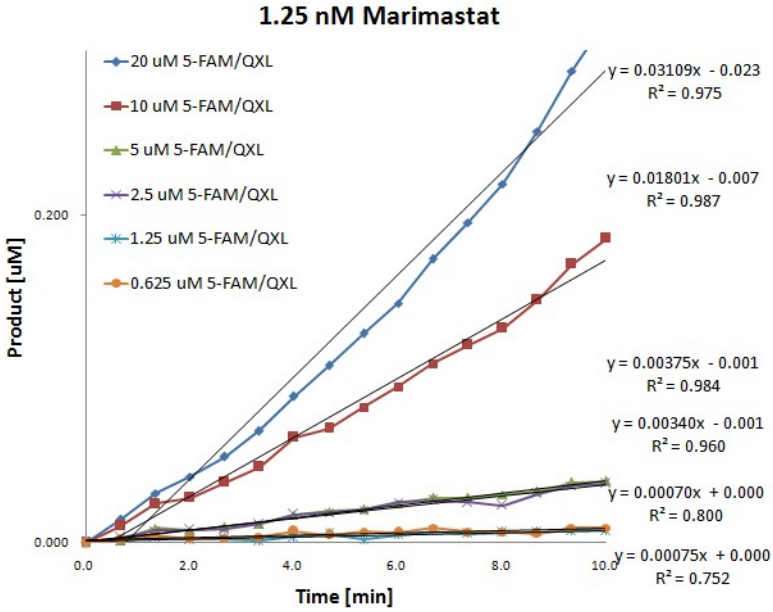

Figure: Velocities for MMP-2 enzyme kinetics experiments

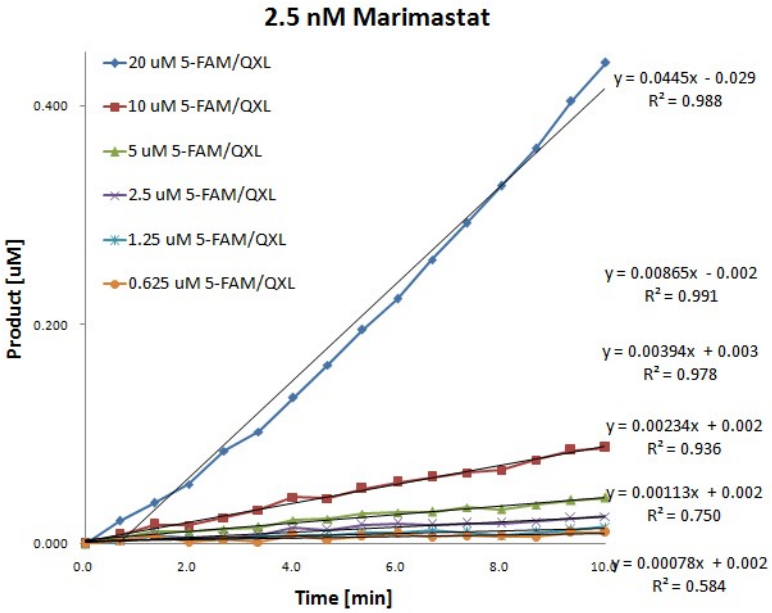

Figure: Velocities for MMP-2 enzyme kinetics experiments

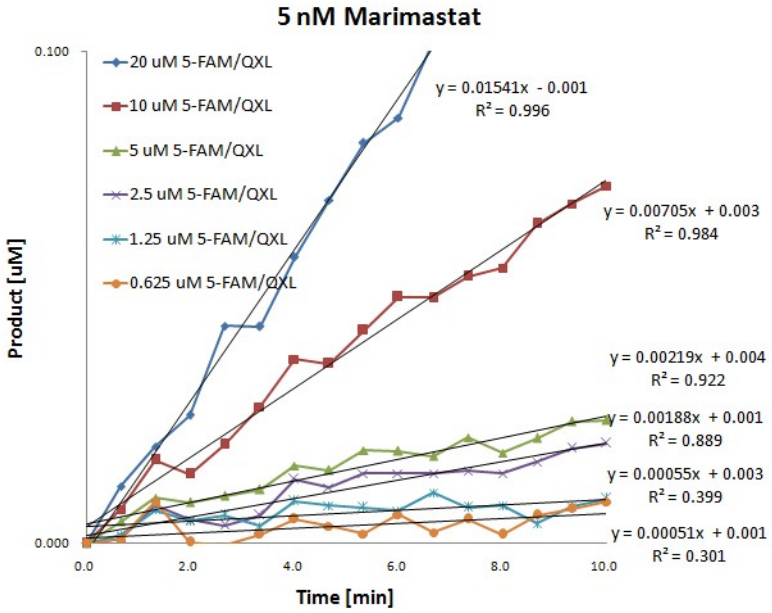

Figure: Velocities for MMP-2 enzyme kinetics experiments

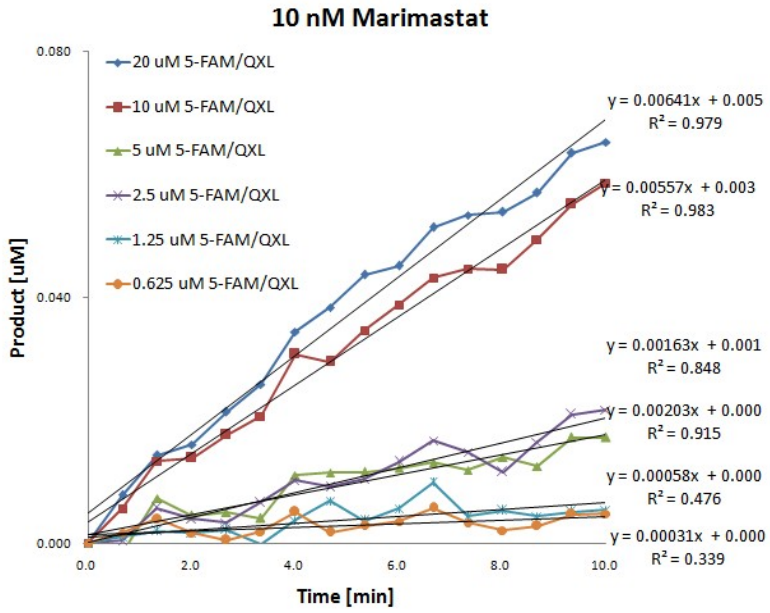

Figure: Velocities for MMP-2 enzyme kinetics experiments

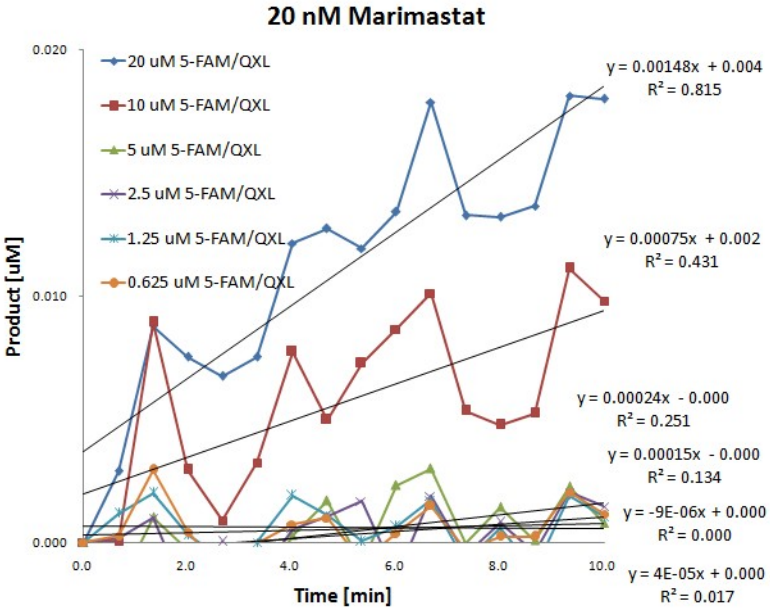

Figure: Velocities for MMP-2 enzyme kinetics experiments